November 19, 2000

AASERT

FINAL REPORT

FILM COOLING IN A PULSATING WALL JET

EXPERIMENTS, NUMERICAL SIMULATION, AND STABILITY THEORY
A Final Report on an AASERT Augmentation Grant entitled:

# THE TURBULENT WEAK WALL-JET

M.D. Zhou and I. Wygnanski

Department of Aerospace and Mechanical Engineering
The University of Arizona
Tucson, AZ 85721

## Introduction

Turbulent wall jets have many important engineering applications. Much effort has been spent to investigate the plane turbulent wall jet without external stream (Launder and Rodi 1981,1983, Katz et al 1992, Wygnanski et al 1992) and with a relatively slow external stream (Zhou and Wygnanski 1993, Zhou et al 1996). However, many engineering applications seem to be described better by a wall jet embedded in a uniform stream of comparable velocity (the weak wall jet), for example, the cooling turbine blades and the flows over a wing equipped with a slotted flap (Fig.1) represents such flows. The recently developed technique for separation control by periodic blowing/suction on the flap also belongs to category (Fig.2). Thus, it is important to provide a better understanding of the development of these flows. For example: the possibility of flow similarity, normalization of the mean velocity fields, scaling laws for the governing parameters, as well as the various responses to external excitations. This report represents but a single facet of the general effort endeavoring to use the wall jet for boundary layer control, film cooling and the exertion of force on a body through the use of what is commonly known as the Coanda Effect.

# REPORT DOCUMENTATION PAGE



AFRL-SR-BL-TR-00-

0803

| 1. AGENCY USE ONLY (Leave blank) | 2. REPORT DATE | 3. REPORT TYPE AND DATES COVERED |
|---|---|---|
| | 11/22/00(REVISED) | Final Technical (7/1/96-2/29/00) |

**4. TITLE AND SUBTITLE**

An AASERT Grant in support of : Film Cooling with a Forced Turbulent Wall Jet

**5. FUNDING NUMBERS**

F49620-96-1-0243

**6. AUTHOR(S)**

Professor Israel Wygnanski

**7. PERFORMING ORGANIZATION NAME(S) AND ADDRESS(ES)**

Department of Aerospace and Mechanical Engineering
The College of Engineering and Mines
The University of Arizona
Tucson, AZ 85721

**8. PERFORMING ORGANIZATION REPORT NUMBER**

**9. SPONSORING / MONITORING AGENCY NAME(S) AND ADDRESS(ES)**

AFOSR/NA
801 N. Randolph St Room 732
Arlington, VA 22203-1977

**10. SPONSORING / MONITORING AGENCY REPORT NUMBER**

**11. SUPPLEMENTARY NOTES**

**12a. DISTRIBUTION / AVAILABILITY STATEMENT**

Approved for Public Release - Distribution is Unlimited

**12b. DISTRIBUTION CODE**

**13.**

Turbulent wall jets have many important engineering applications. Much effort has been spent to investigate the plane turbulent wall jet without external stream (Launder and Rodi 1981,1983, Katz et al 1992, Wygnanski et al 1992) and with a relatively slow external stream (Zhou and Wygnanski 1993, Zhou et al 1996). However, many engineering applications seem to be described better by a wall jet embedded in a uniform stream of comparable velocity (the weak wall jet), for example, the cooling turbine blades and the flows over a wing equipped with a slotted flap (Fig.1) represents such flows. The recently developed technique for separation control by periodic blowing/suction on the flap also belongs to category (Fig.2). Thus, it is important to provide a better understanding of the development of these flows. For example: the possibility of flow similarity, normalization of the mean velocity fields, scaling laws for the governing parameters, as well as the various responses to external excitations. This report represents but a single facet of the general effort endeavoring to use the wall jet for boundary layer control, film cooling and the exertion of force on a body through the use of what is commonly known as the Coanda Effect.

**14. SUBJECT TERMS**

**15. NUMBER OF PAGES**
3

**16. PRICE CODE**

| 17. SECURITY CLASSIFICATION OF REPORT | 18. SECURITY CLASSIFICATION OF THIS PAGE | 19. SECURITY CLASSIFICATION OF ABSTRACT | 20. LIMITATION OF ABSTRACT |
|---|---|---|---|
| UNCLASSIFIED | UNCLASSIFIED | UNCLASSIFIED | UNLIMITED |

**Experimental set up.**

The experiments were carried out in the 3'x2' close-loop wind tunnel in the AME Department in University of Arizona. It was equipped with an adjustable roof that enabled it to achieve the condition of zero pressure gradient.

The wall-jet facility was mounted at the bottom of the test section (Fig.3). The nozzle of the jet was flush with the floor of the wind tunnel and the nozzle width could be adjusted by a pair of micro-metric jackscrews attached to the upper lip of the nozzle. The air-flow was provided by a centrifugal blower powered by a frequency-controlled AC motor. A loudspeaker was mounted in the plenum chamber upstream of a set of screens and a honeycomb. The temperature of the wind tunnel flow and of the jet flow were controlled and monitored independently so that the temperature could be kept constant within accuracy of 0.1 degree C.

The instantaneous velocity signals were measured using a constant temperature hot wire anemometer manufactured by AA Lab System. The signals were processed digitally in order to obtain statistical quantities such as mean velocities, turbulence intensities and spectra, as well as phase-locked or temporal pattern recognition and matching.

**Results and discussions**

1. Some general features categorizing the wall jets.

   a. Strong wall jet and weak wall jet.

   From the previous experiments on wall jets in the stagnant surroundings (Wygnanski et al. 1992), all mean velocity profiles could be normalized by a length scale of $Y_2$ and a velocity scale of $U_m$. Later experiments on wall jets in an external stream (Zhou and Wygnanski 1993) indicated that the mean velocity profiles can also be collapsed onto a single curve provided two length scales and two velocity scales are used for the inner and outer layers. This idea worked out, even when considerations of the equations of motion suggested otherwise, as long as the ratio $U_\infty/U_j$ is less than 0.5. In order to demonstrate this limitation, only one length scale is used to normalize the entire wall jet as shown in Fig.4. The major difference between the flows with $U_\infty/U_j$ $<0.5$ and $U_\infty/U_j >0.5$ appears since the ratio $Y_m/Y_2$ is constant at all values of x for the former case but not for the latter. Thus, we defined a strong wall jet as one having $U_\infty/U_j <0.5$ and a weak wall jet for which $U_\infty/U_j>0.5$.

   b. Weak wall jet, type 1 and type 2.

   Twelve sets of data representing the weak wall jet in absence of pressure gradient and surface curvature were measured and summarized in table 1.

**Table 1. Measured data for weak wall jet**

| | $U_\infty$(m/s) | $U_j$(m/s) | b(mm) | $Re_j$ | $U_\infty/Uj$ | R | θ(mm) | $U_\infty^2\theta/U_j^2b$ | Hz |
|---|---|---|---|---|---|---|---|---|---|
| Set A | 9.2 | 15.4 | 7 | 7200 | 0.6 | 0.25 | 0.47 | 0.024 | |
| B | 12.5 | 20.8 | 5 | 6900 | 0.6 | 0.25 | 0.47 | 0.030 | |
| C | 19.5 | 32.8 | 5 | 11000 | 0.59 | 0.26 | 0.47 | 0.034 | |
| D | 11.3 | 15.3 | 7 | 7100 | 0.74 | 0.15 | 0.47 | 0.036 | |
| E | 12.3 | 14.5 | 7 | 6800 | 0.85 | 0.081 | 0.47 | 0.043 | |
| F | 14.3 | 15.5 | 7 | 7200 | 0.92 | 0.042 | 0.47 | 0.058 | |
| G | 19.5 | 21 | 5 | 7000 | 0.93 | 0.036 | 0.47 | 0.085 | |
| H | 18.4 | 15 | 7 | 7000 | 1.23 | -0.1 | 0.47 | 0.097 | |
| I | 17.3 | 18.3 | 4 | 4900 | 0.95 | 0.026 | 4.9 | 1.02 | |
| J | 12.3 | 15.3 | 7 | 7100 | 0.8 | 0.11 | 0.47 | 0.04 | 106 |
| K | 17.3 | 18.3 | 4 | 4900 | 0.95 | 0.026 | 4.9 | 1.02 | 104 |
| L | 17.3 | 18.3 | 4 | 4900 | 0.95 | 0.026 | 4.9 | 1.02 | 75 |

A typical wall jet in streaming flow is embedded in a boundary layer whose relative thickness and momentum deficit may be of significance relative to the initial width of the wall jet and its momentum. Thus a weak wall jet is embedded in a wake (a region of momentum deficit) that is easily distinguishable by the perseverance of a velocity minimum in the mean velocity profiles. Such a minimum is clearly visible in the upstream region near the blowing slot, however, there are two possible developments downstream. In the first case (type 1) the velocity minimum disappears and the local mean velocity profiles are similar to those observed in a strong wall jet (Fig.5a). In the second case, the disappearance of the velocity minimum is coupled with the disappearance of the velocity maximum that characterizes the wall-jet. A distorted boundary layer profile containing a significant wake component is generated and it relaxes further downstream to an ordinary, flat plate turbulent boundary layer (Fig.5b).

The major parameter distinguishing these two classes of flow is the ratio of the momentum lost in the upstream boundary layer to the momentum added by the jet. When the ratio of $U_\infty^2\theta/U_j^2b$ <0.036, the momentum lost in the upstream flow is not large enough to cause a major change in the wall jet characteristics downstream, otherwise he momentum added by the jet is insufficient to overcome the momentum lost by the upstream flow. Thus, a study of a weak wall jet has to distinguish between these various categories.

c. The border of far field and near field.

As can be expected from Fig.5, the flow in the upstream region (the near field where the velocity minimum exists) will have entirely different characteristics from the far,

downstream region. In the near field, the mean velocity profiles consisted of three vortical layers: first is the new boundary layer region closest to the wall, above it is a shear layer (having an opposite sign of vorticity) separating the jet flow from the upstream (usually much thicker) boundary layer which represents the third vortical layer. Far downstream, the type 1 weak wall-jet contains only two vortical layers of opposite sign, while the far field of the type 2 wall-jet reminds one of a distorted boundary layer. Thus, flow similarity arguments and their associated scaling laws, have to consider each category separately.

The border between the near and far fields is shown in Fig.6, where the dimensionless streamwise location for the velocity minimum to disappear $\xi_{dis.}$ is shown as a function of the momentum ratio, Jvis/Jinv, where

$$\xi = XJ_{inv} / \nu^2$$

$$J_{inv} = U_j(U_j - U_\infty)b$$

$$J_{vis} = U_j(U_j - U_\infty)b - U_\infty^2\theta$$

This ratio represents a dimensionless difference between the momentum added by the jet and the momentum lost by the boundary layer.

2. Similarity and scaling parameters appropriate to the far field of weak wall jet labeled as type1.

Since stability characteristics depend on the form of the mean velocity distribution, the far field of the weak wall jet (type1) consisting of two vortical layers resembles the strong wall jet. The outer layer represents a mixing region whose width may serve as reference length-scale to be used for dimensionless normalization, while the maximum velocity difference between the free stream and the maximum velocity observed in the jet may serve as a velocity-scale for the purpose of normalization. The inner layer is a boundary layer region and can be normalized by its thickness while its velocity scale is the maximum velocity (because of the non-slip condition. The collapse of all the mean velocity profiles measured in the far field of type 1 weak wall jet is shown in Fig.7. These results look quite similar to the results obtained for the strong wall jet (Zhou and Wygnanski 1993), however, streamwise development of the major parameters is not the same as might have been expected from Fig.4.

The streamwise behavior of the inner layer length-scale, $Y_{max}$, is shown in Fig.8. The scaling is similar to that of the strong wall jet provided the momentum involved is $J_{vis}$ that considers the effect of the viscous losses. The power-law governing the strong wall jet is thus shown by dashed line in Fig. 8 for comparison. The inner layer of the weak wall jet spreads out somewhat less quickly than it does for the strong wall jet. The scaling of $Y_2$ and $U_{max}$ are shown in Fig.9 and 10 respectively where $R=(U_J-U_\infty)/(U_J+U_\infty)$. $Y_2$ represents the distance of the point in the outer layer where the dimensionless velocity, $(U-U_\infty)/(U_{max}-U_\infty)=0.5$. All these figures suggest that the weak wall jets develop more

moderately with increasing X than the strong wall jets. This trend is reasonable if we consider the dimensionless streamwise distance $\xi$ as representing a product of two Reynolds numbers. One is the jet Reynolds number and the other, a Reynolds number based on the streamwise distance from the nozzle and the velocity difference between jet and the free stream. For identical jet Reynolds number and streamwise distance, the streamwise Reynolds number is smaller for the weak wall jet than in the strong one. The scaling of the wall shear stress is shown in Fig.11, provided the same scaling parameters as in the strong wall jet are applied. However, a much better collapse of all the data is achieved by considering the Reynolds number effect (Fig.12). The physical reason for this is discussed below.

Generally speaking, the wall jet in an external stream, regardless of it being strong or weak, is not a self-similar flow. Such a wall jet has to evolve into a boundary layer at an appropriate downstream distance. In this sense, the proper scaling laws will depend on this distance that determines how far away they presently are from the final equilibrium states. The scaling laws for the strong wall jets presented by Zhou and Wygnanski 1993 are limited by the velocity ratio between free stream and the jet exit velocity that is less than 0.5. These strong wall jets are farther away from the equilibrium boundary layer than the weak wall jets discussed presently and thus the influence of the boundary layer is not apparent. Therefore, the applicable governing parameters are the jet momentum, fluid viscosity and the velocity ratio $U_\infty/Uj$. However, in the weak wall jets, some of the losses in the upstream and in the developing new boundary layer have to be taken into account. It can be seen (Fig.4) that when $U_\infty/Uj = 0.59$, the mean velocity lost its similarity to the other wall jets having $U_\infty/Uj < 0.5$. Apparently, $Y_m/Y_2$ in the former case increases significantly thus affecting the decay of $U_m$. It is reasonable to consider the scaling laws for the weak wall jets by adding a parameter representing the boundary layer losses in such flows. By considering the wall shear stress in the boundary layer, the parameters associated with the Reynolds number in the weak wall jet can be determined.

In a laminar boundary layer in the absence of pressure gradient or curvature, we have:

$$\delta = 5.0\frac{x}{\sqrt{\mathrm{Re}_x}} \qquad C_f = \frac{0.664}{\sqrt{\mathrm{Re}_x}}$$

While for turbulent boundary layers under the same conditions,

$$\delta = 0.37\frac{x}{\sqrt[5]{\mathrm{Re}_x}} \qquad C_f = \frac{0.0592}{\sqrt[5]{\mathrm{Re}_x}}$$

Obviously, Reynolds number is the dominant parameter expressing the boundary layer behavior. However, in weak wall jets the definition of Reynolds number should be derived from the definition of $J_{vis}$. Since $J_{vis}$ represents the difference between the jet momentum and the momentum lost in the upstream boundary layer, the analogous difference between the jet efflux the flow rate loss in the upstream boundary layer should also be considered in the definition of the present Reynolds number, i.e.

$$\mathrm{Re}_{jvis} = (U_j b - U_\infty \delta^*)/\nu$$

The second consideration is that the power of the Reynolds number will be different for different flows. Thus, the power is determined by the best fit to the data. The results show that the powers of Reynolds number for scaling of $Y_m$ and $Y_2$ are negligible, i.e. the expression is the same as in the strong wall jet. The power for scaling of $U_m$ should be non-zero but it is small as can be deduced from Fig.10. However, the power for scaling the wall shear stress is significant and this scaling law can be expressed by the following (Figure 12):

$$\frac{\tau_w R^{1.5}}{\rho}\left(\frac{\nu}{J_{vis}}\right)^2 \mathrm{Re}_{jvis}^{2.5} = g(\xi)$$

3. Similarity and scaling of the flow in the near field of the weak wall jet.

It is obvious (Fig.5) that the extent of the near fields in the type 1 weak wall jets are quite short, thus only the near field profiles of type 2 weak wall jet are considered presently. Apparently, the mean velocity profiles in the near field are composed mostly of three vortical layers, two resembling mixing layers and one representing the development of the new boundary. Thus, it is reasonable to normalize the mean velocity profiles with three velocity-scales and three length-scales. Such normalized mean velocity profiles are shown in Fig.13. The collapse of the data onto a single curve is very good although some scatter may be noticed in the boundary layer region.

The evolution of $Y_{max}$, $Y_2$, $Y_3$, $U_{max}$ and $U_{min}$ as well as the wall shear stress with downstream distance are shown in Fig.14 to 19, where $Y_2$ is the distance from the wall of the point in the middle layer where the normalized velocity $(U-U_{min})/(U_{max}-U_{min})= 1/2$ while $Y_3$ is the corresponding distance from the wall to a similar point in the outer layer [i.e. where $(U-U_\infty)/(U_\infty-U_{min})=1/2$]. Although we had only a limited number of data points to compare the type 2 weak jets, the collapse onto a single curve is impressive. One interesting point here is that the jet momentum J that collapses the data is the inviscid $J_{inv}$ instead of the viscous one, $J_{vis}$. The explanation for this behavior may stem from the following arguments. The near field development is accomplished in a short streamwise distance where the mean velocity profile is dramatically altered. Thus, for the same reason as in the rapid distortion theory, this short process could be regarded as inviscid. Surprisingly however, the dimensionless parameters here are identical to the far field parameters describing the type 1 weak wall jet except for dimensionless $U_{min}$ (where R is raised to the power of 1.5) and wall shear stress(where R is raised to the power of 2).

4. On the far field of type 2 weak wall jet.

It can been seen from Fig.5b that the far field of a type 2 weak wall jet is represented by a distorted boundary layer. The mean flow is dominated by the upstream boundary layer that is disturbed by a wall jet that adds some momentum to the flow. The added momentum is not strong enough to generate a wall-jet-like flow as it does in the type 1, so the flow recovers to a regular boundary layer not far away from the jet exit. Thus, no matter how one chooses the velocity and the length scales, the mean velocity profiles do not collapse. This lack of similarity is the common characteristics of the non-equilibrium boundary layers. However, it may be meaningful to observe the general tendency of its streamwise development. Consequently the streamwise distributions of the shape factors in the weak wall jet are shown in Fig.20. To begin with, all of the values are lower than the well known equilibrium value of 1.4 because the jet makes the profiles fuller than in a corresponding simple boundary layer. The shape factors increase gradually in the streamwise direction and eventually approach the same asymptotic value existing in an equilibrium boundary layer. For comparison, a curve representing a typical type 1 weak wall jet is also shown in the figure.

5. Forced weak wall jet.

The above discussions are based on the common features of the weak wall jet. In order to study the behavior of weak wall jet under external excitation, we intended to choose a typical weak wall jet that is as close as possible to the one observed when separation control is required. From Fig.1 and 2, the flow should be a type 2 weak wall jet with a fairly thick initial boundary layer. Thus the upstream boundary layer was artificially thickened and is much thicker than the naturally observed one by Weidemann in 1996. The mean velocity profiles as well as the turbulent energy distributions (u component) are shown in Fig 21. The major region of measurement is in the near field.

A careful observation of the mean velocity profiles and the turbulence energy distribution suggest the existence of three instability modes in the flow. From x/b=10 to 30, there are clearly three peaks in the turbulence energy distribution corresponding to the three shear layers. The locations of intensity peaks do not correspond exactly to the locations of the maximum strain rate in the mean velocity profiles. This is believed to be attributed to the strong diffusion existing in the near field. Anyway, three possible frequency should be considered for excitation of the three individual instability modes. A systematic search was carried out experimentally for maximum response in the three individual regions. Only two particular frequencies, 104Hz and 75Hz, were found to have identifiable response. The influence of forcing on the global growth of the wall jet is shown in Fig.22. The flow with external forcing results in a thicker layer but almost the same growth rate over most of the region of interest implying that forcing enhanced the upstream mixing very near to the jet exit. Furthermore, the 75Hz forcing resulted in a stronger thickening of the layer than the 104 Hz excitation. The influence of forcing on the skin friction is shown in Fig.23. The maximum skin friction reduction caused by a

forcing level of 7.5% was 25 %, and it is caused by 104 Hz excitation. No identifiable influence on skin friction was detected under 75Hz forcing.

The reasons for the abovementioned phenomena were exposed by the phase-locked ensemble averaging technique and the temporal pattern matching technique. The amplitude and phase distributions across the layer during forcing at the frequency of 104 Hz were obtained by the phase locking and ensemble averaging of the data and are shown in Fig.24. Apparently, 104Hz is the instability frequency of the inner layer (or the wall layer) mode, that caused a strong peak close to the wall only. This peak disturbance produced a strong mixing and reduced the mean velocity slope in the wall region reducing the skin friction as well. The phase locked amplitude distribution under 75 Hz forcing is shown in Fig.25a. A strong peak in the middle region of the layer can be seen in particular from x/b=25 to 38. Obviously, it represents the instability frequency of the middle region. No outer-layer instability mode was found to date. However, it was noticed that in the outer layer, there existed very strong phase jitter which might smear out the coherent waves although the latter could be identified from the instantaneous waves. Thus, the temporal pattern matching technique (Zhou et al 1996) was applied to the same data under 75Hz forcing. The coherent amplitude distributions obtained in this manner are plotted in Fig.25b. Now, it becomes clear that there existed another intensity peak in the outer layer that is comparable to that in the middle layer region. It means that the instability frequency of the outer layer is very close to that in the middle layer so that the two modes become strongly coupled. This explains why the 75Hz had stronger influence on the global thickness of the wall jet than 104Hz.

## 6. Discussion.

a. <u>On the criterion to identify strong and weak wall jets.</u>

A weak wall jet is not merely identified by the existence of a velocity minimum in its mean-velocity profiles. An example is shown in Fig.26 where this definition does not hold. The data represents a strong wall jet having $U_\infty/Uj < 0.5$ and the scaling of its velocity and length scales collapse well according to the scaling laws of the strong wall jet (Zhou and Wygnanski 1993). However, it is embedded in an artificially thickened boundary layer and there are obviously velocity minima in the upstream region. Thus, the appearance of velocity minimum in the mean velocity profiles should not be regarded as being a characteristic of the weak wall jet.

b. <u>On the similarity between wall jets and wall wakes.</u>

In order to compare the weak wall jet with the wall wake, the data measured behind three wake generators in a boundary layer with zero pressure gradient were used (Zhou and Squire 1981). Model A was a blunt tail strut. Model B was the same strut as model A but with additional tail filler to form a thick airfoil. Model C was a flat plate with the same drag as model B. The mean velocity profiles in the near field look very similar to those in the near field of a weak wall jet. The same normalization procedure with three velocity scales and three length scales was tested to these profiles. The normalized mean

velocity profiles are shown in Fig.27 and are very close to those of the weak wall jets. However, there is no way to apply the same scaling technique to the streamwise development of the wall wakes. One of the difficulties was the ambiguity of the equivalent 'jet momentum'. The other problem is that the turbulent wake structure that has apparently a strong influence on the growth of the wall wake.

**Summary**

1. A weak wall jet is a wall jet with the ratio of external stream velocity to jet velocity in excess of 0.5. According to the ratio of momentum loss in the upstream boundary layer to the added jet momentum, the weak wall jet can be further divided into two types. The type 1 develops into a strong wall-jet-like flow in the far field, while the type 2 jet develops into a distorted boundary layer.

2. The mean velocity profiles in the near field can be collapsed with three length scales and three velocity scales. Those in the far field of type 1 weak wall jet can be collapsed with two length scales and two velocity scales. However, no similarity can be found in the far field of the type 2 weak wall jets.

3. The scaling laws of the length and velocity scales are different from the strong wall jet, although the dimensionless parameters are similar. One of the main differences represent the influence of the momentum loss in the upstream boundary layer that has to be taken into account in the weak wall jet. Another major difference is that the weak wall jet develops much slower than a strong wall jet.

4. The data with forcing showed that there are three possible instability modes, however, the two modes corresponding to the outer and the middle shear layers are strongly coupled so that the same forcing frequency strongly thickened the wall jet. The inner layer mode which causes a strong peak of coherent amplitude very close to the wall reduced the skin friction by as much as 25% in our experiment.

5. The normalized mean velocity distribution of the wall wakes can approximately be collapsed with the profiles in the near field of the weak wall jet. However, there is no way to scale their streamwise development since the turbulent structure in the wall wake has strong influence on their growth.

**List of figures**

Fig.1. The weak wall jet over a typical slotted flap.

Fig.2. The weak wall jet over a deflected flap of a NASA 0015 airfoil with blowing and oscillation.

Fig.3. A schematic diagram of the wall-jet facility.

Fig.4. The wall jet normalized with two velocity scales and one length scale.

Fig.5. Two types of weak wall jets.
(a) Weak wall jet type 1.
(b) Weak wall jet type 2.

Fig.6. Border of near field and far field of the weak wall jets.

Fig.7. Mean velocity profiles in the far field of type 1 weak wall jet normalized with two velocity scales and two length scales.

Fig.8. Scaling of Ymax in the far field of type 1 weak wall jet.

Fig.9. Scaling of Y2 in the far field of type 1 weak wall jet.

Fig.10. Scaling of Umax in the far field of type 1 weak wall jet.

Fig.11. Scaling of skin friction in the far field of type 1 weak wall jet without considering the Reynolds number effect.

Fig.12. Scaling of skin friction in the far field of type 1 weak wall jet after considering the Reynolds number effect.

Fig.13. Mean velocity profiles in the near field of weak wall jets normalized with three velocity scales and three length scales.

Fig.14. Scaling of Ymax in the near field of type 2 weak wall jet.

Fig.15. Scaling of Y2 in the near field of type 2 weak wall jet.

Fig.16. Scaling of Y3 in the near field of type 2 weak wall jet.

Fig.17. Scaling of Umax in the near field of type 2 weak wall jet.

Fig.18. Scaling of Umin in the near field of type 2 weak wall jet.

Fig.19. Scaling of skin friction in the near field of type 2 weak wall jet.

Fig.20. Streamwise development of the shape factor in the type 2 weak wall jet.

Fig.21. Mean velocity and turbulence energy distribution of a selected type 2 weak wall jet (data set I)

Fig.22. Influence of external excitation on the spreading of a weak wall jet (data set I, K and L).

Fig.23. Influence of external excitation on the skin friction Cf (data set K).

Fig.24. Amplitude and phase distributions under forcing at the inner instability frequency obtained by the phase locked ensemble averaging technique (data set K).

Fig.25 Coherent amplitude distribution with forcing at the middle instability frequency (data set L).

a. Amplitude distributions obtained by the phase locked ensemble averaging technique

b. Amplitude distribution obtained by the temporal pattern matching technique.

Fig.26. A strong wall jet embedded in an artificially thickened boundary layer.

Fig.27. The mean velocity profiles of wall wake normalized with three velocity scales and three length scales.

**References**

Launder,B.E. and Rodi,W.: The turbulent wall jet, Prog.Aerospace Sci., Vol.19, pp.81-128, 1981.

Launder,B.E. and Rodi,W.: The turbulent wall jet – measurements and modeling, Ann.Rev.Fluid Mech, Vol.15, pp.429-459, 1983.

Katz,Y.; Horev,E. and Wygnanski,I.: The forced turbulent wall-jet, J.Fluid Mech., Vol. 242, pp.577-609. 1992.

Wygnanski,I.; Katz,Y. and Horev,E.: On the applicability of various scaling laws to the turbulent wall-jet, J.Fluid Mech., Vol. 234, pp.669-690. 1992.

Zhou,M.D. and Squire,L.C.: The interaction of a wake with a boundary layer - Data report. CUED/A-Aero/TR 11, Cambridge University, Engineering Department, 1981.

Zhou,M.D. and Wygnanski,I.: Parameters governing the turbulent wall jet in an external stream. AIAA J. Vol.31, No.5, pp.848-853. 1993.

Zhou,M.D.; Heine,C. and Wygnanski,I.: The effects of excitation on the coherent and random motion in a plane wall jet. J. Fluid Mech. Vol.310, pp.1-37, 1996.

Weidemann,M.S.: The weak wall jet, Master thesis, University of Arizona and Technical University of Berlin, 1996.

# Flap Velocity Profiles

$\alpha=8^o$, $\delta f=30^o$, $R_c=0.2*10^6$

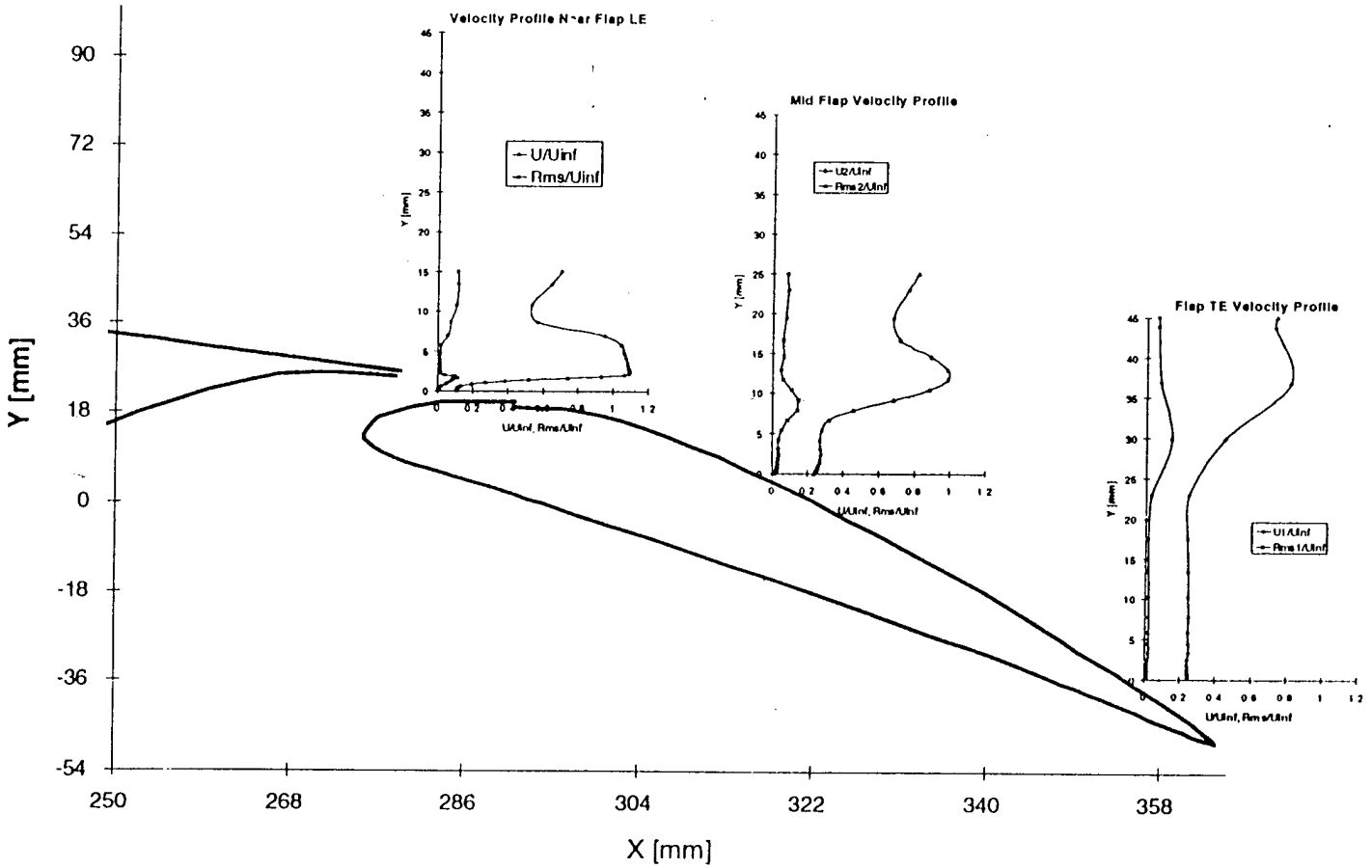


Fig.1. The weak wall jet over a typical slotted flap.

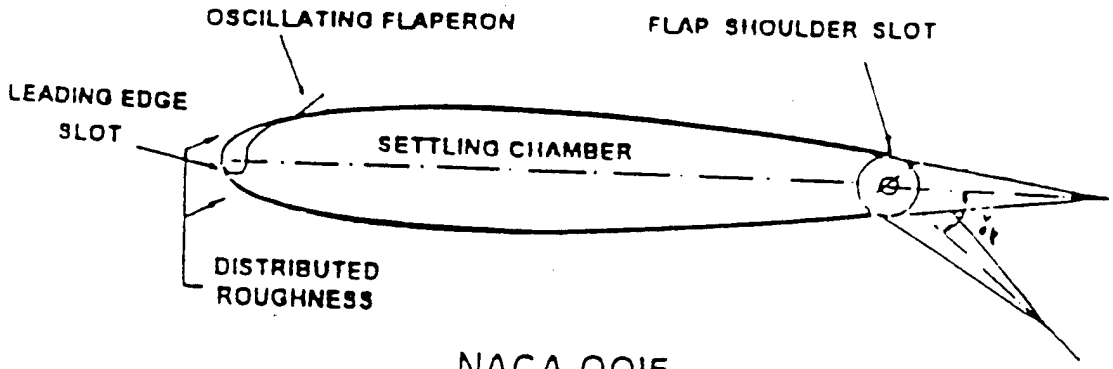


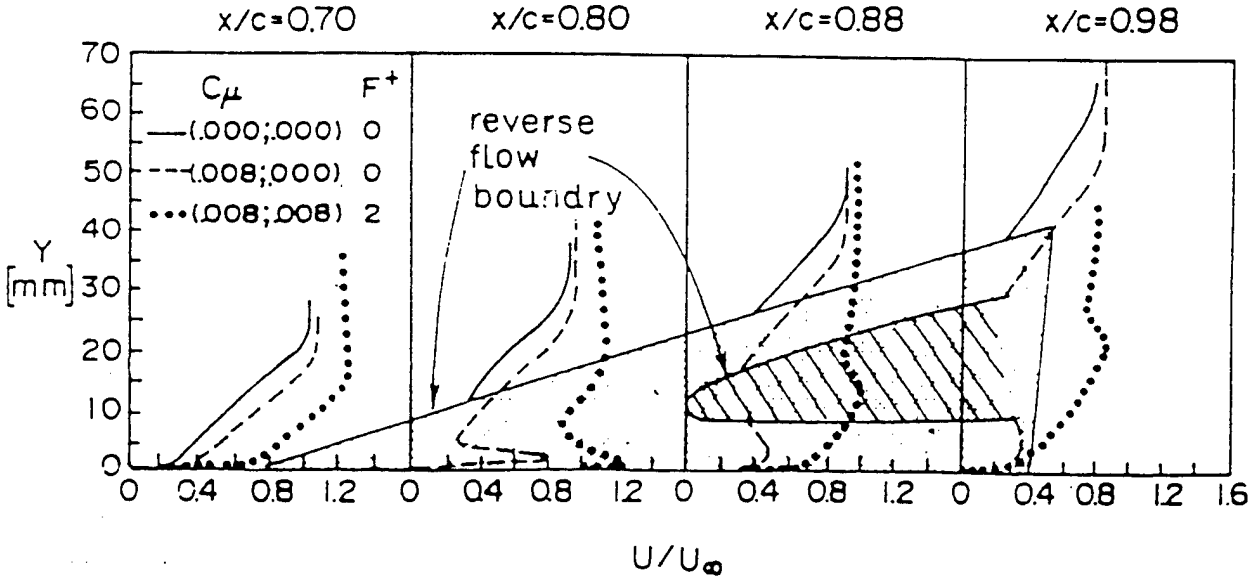


Fig.2. The weak wall jet over a deflected flap of a NASA 0015 airfoil with blowing and oscillation.

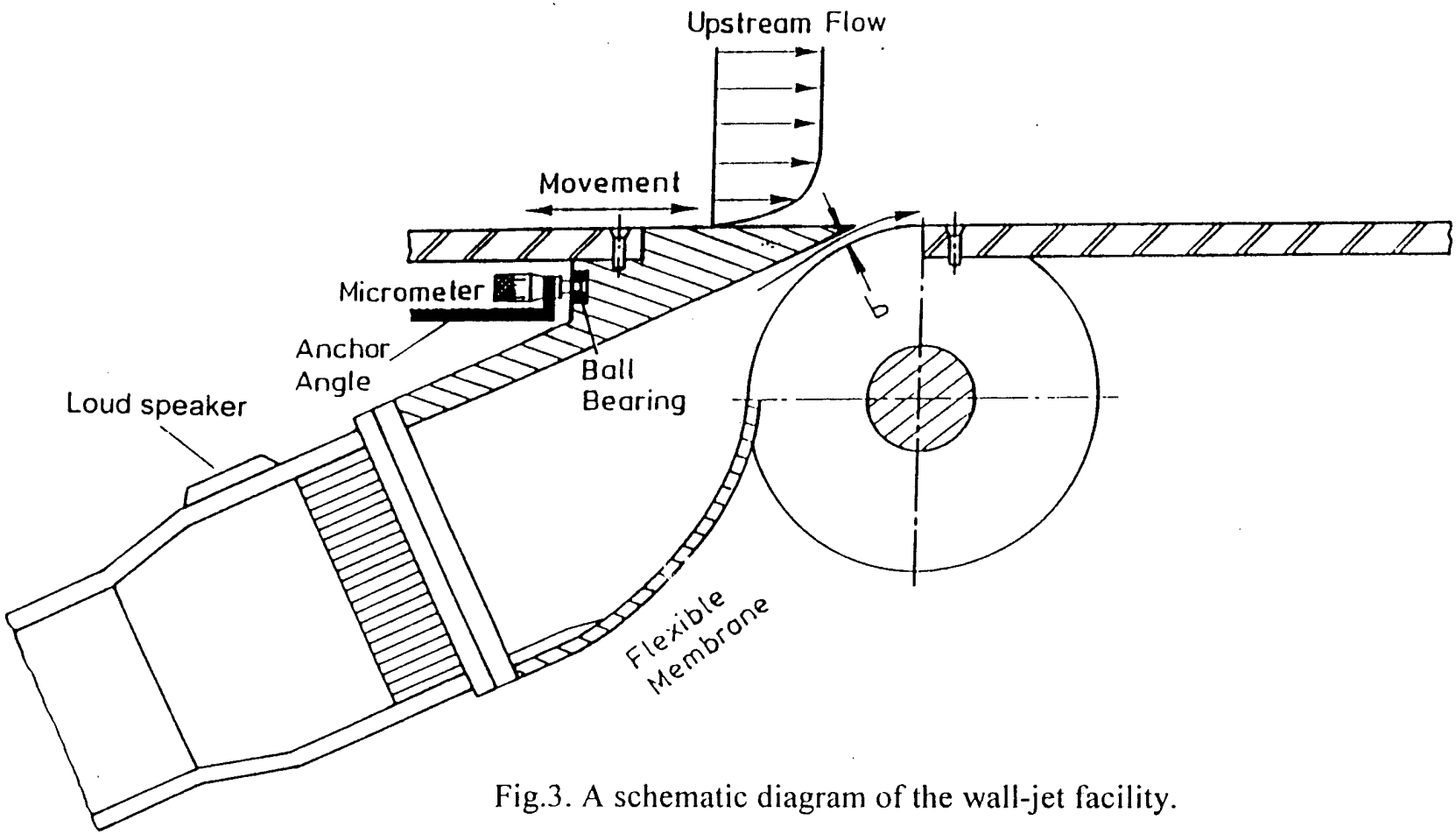


Fig.3. A schematic diagram of the wall-jet facility.

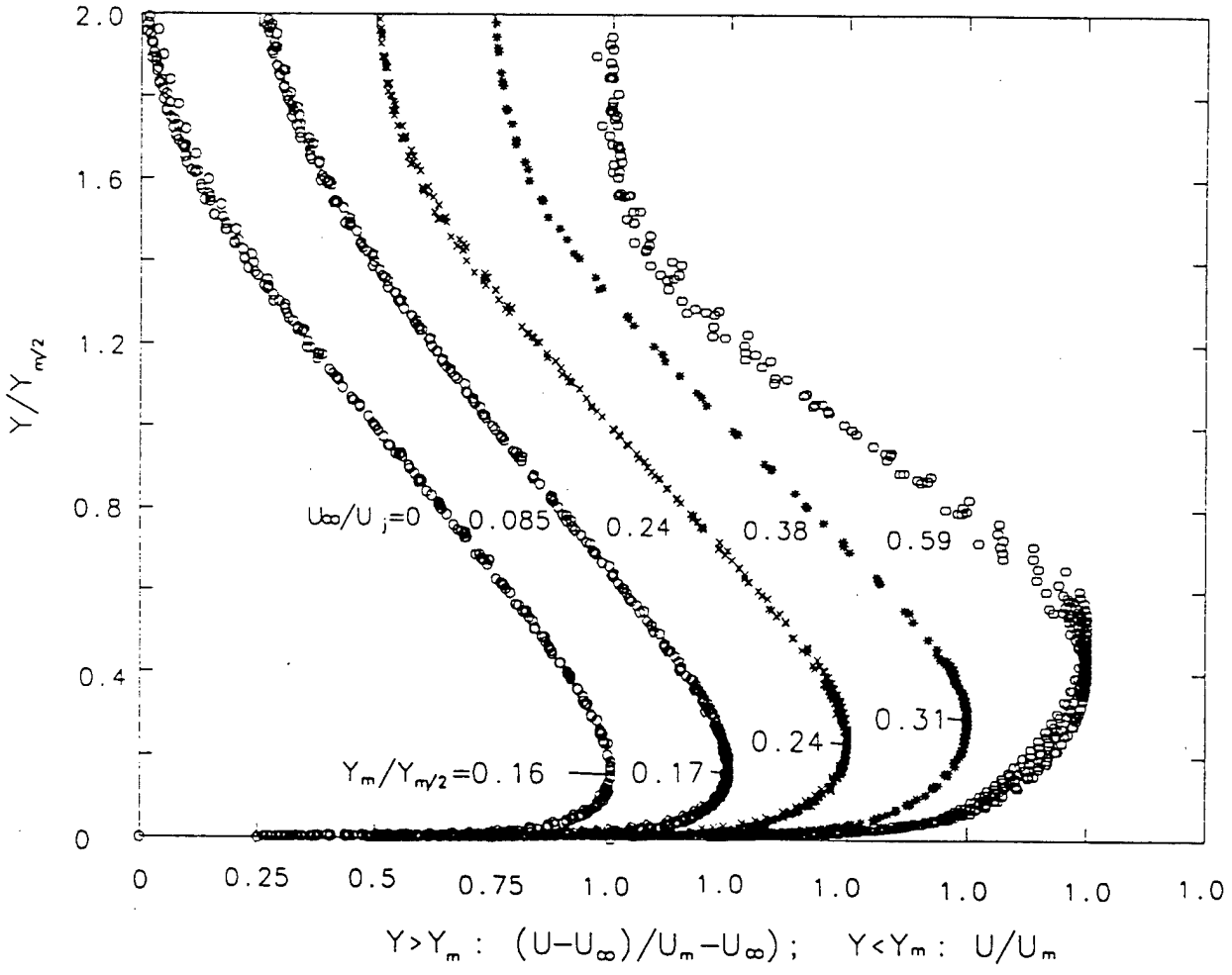


Fig.4. The wall jet normalized with two velocity scales and one length scale.

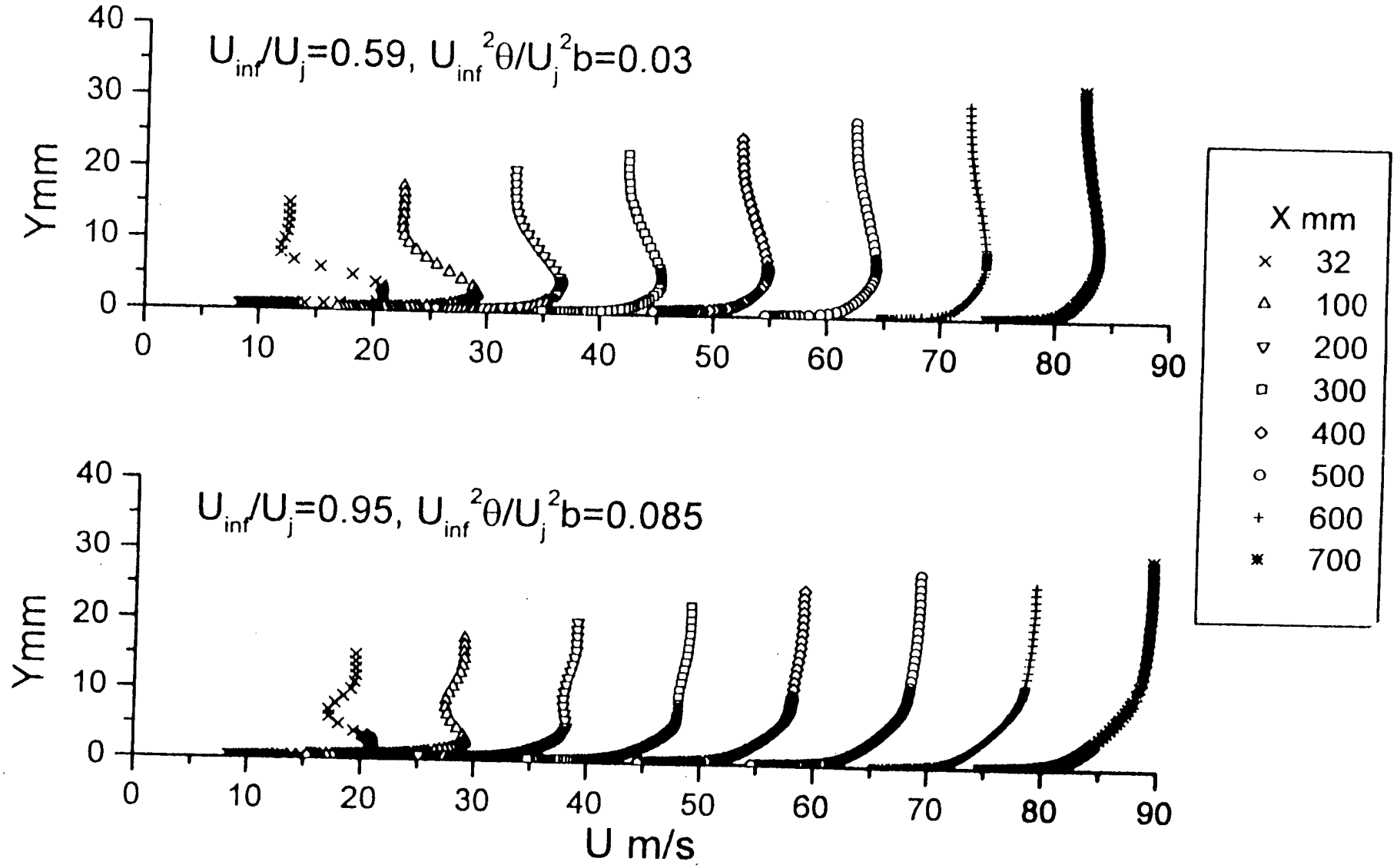


Fig.5. Two types of weak wall jets.
(a)Weak wall jet type 1.
(b) Weak wall jet type 2.

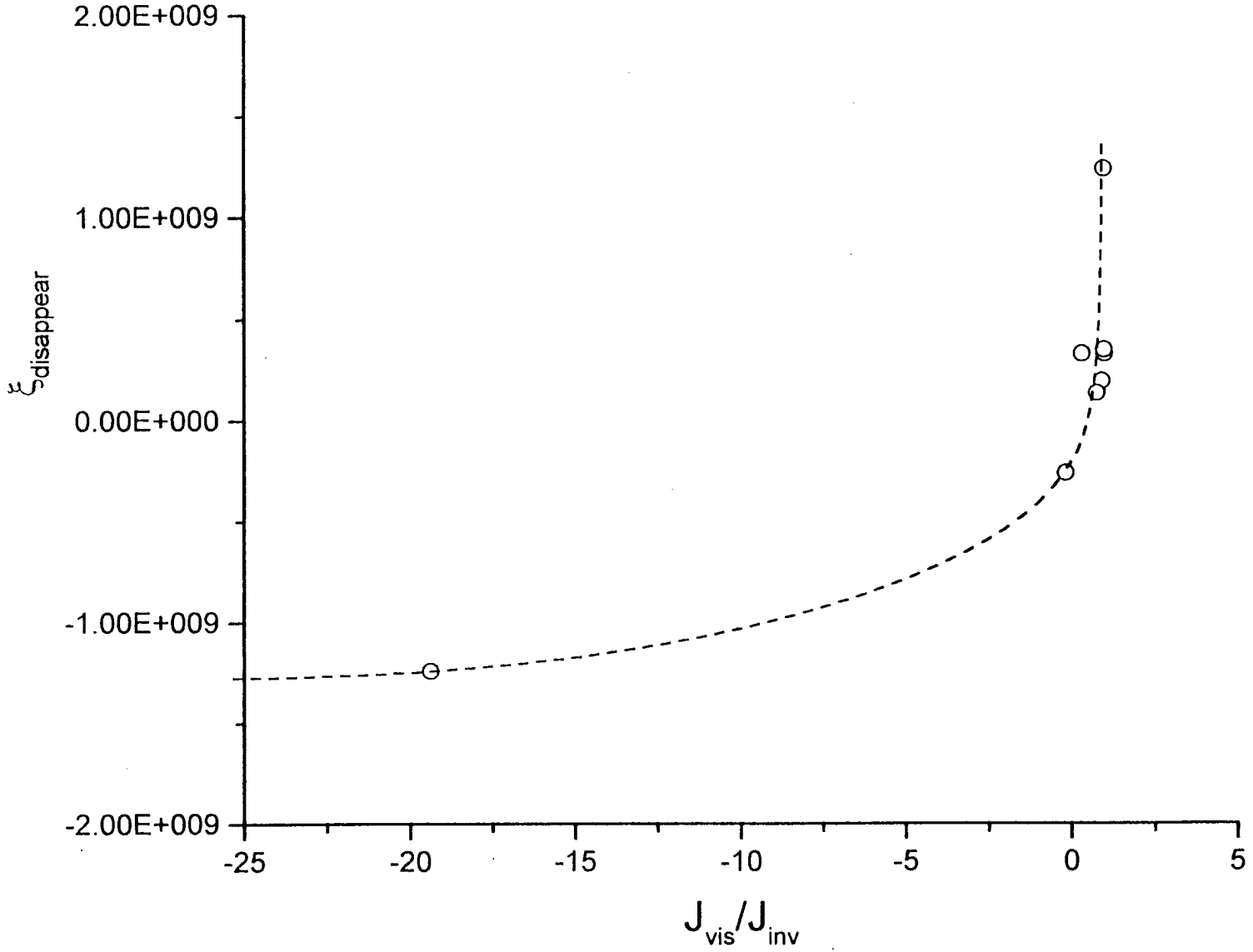


Fig.6. Border ofnear field and far field of the weak wall jet

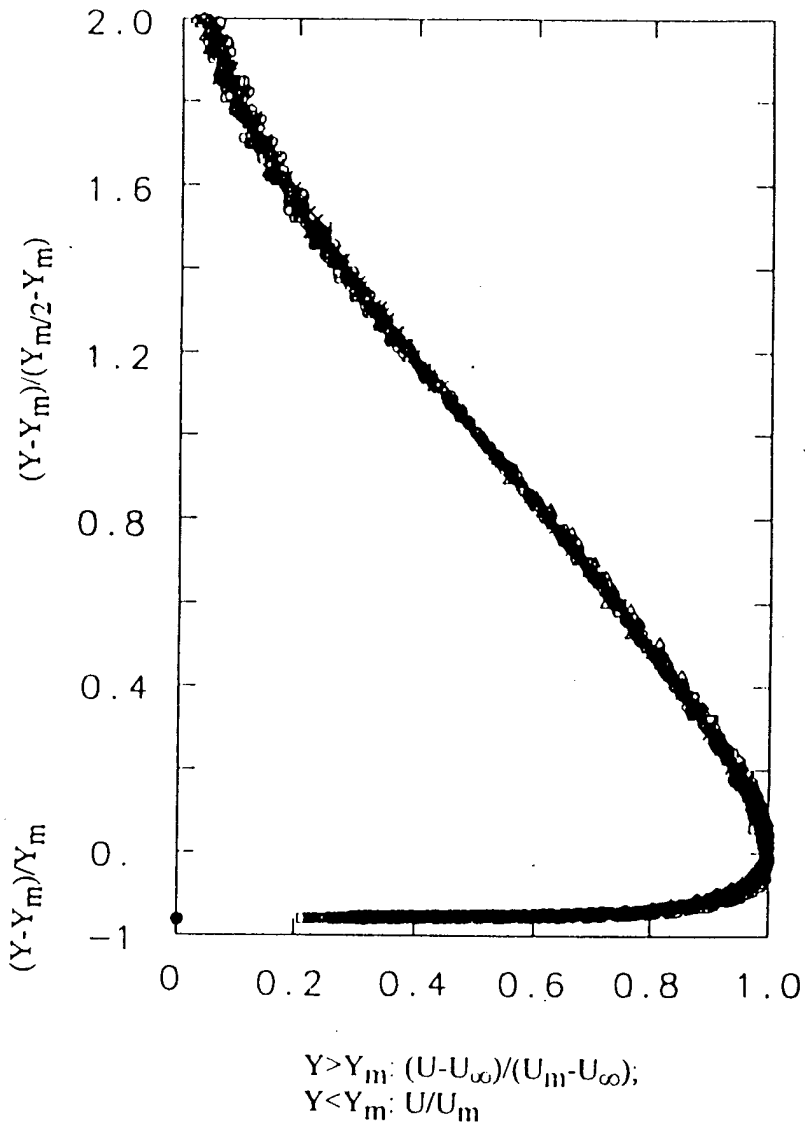


Fig.7. Mean velocity profiles in the far field of type 1 weak wall jet normalized with two velocity scales and two length scales.

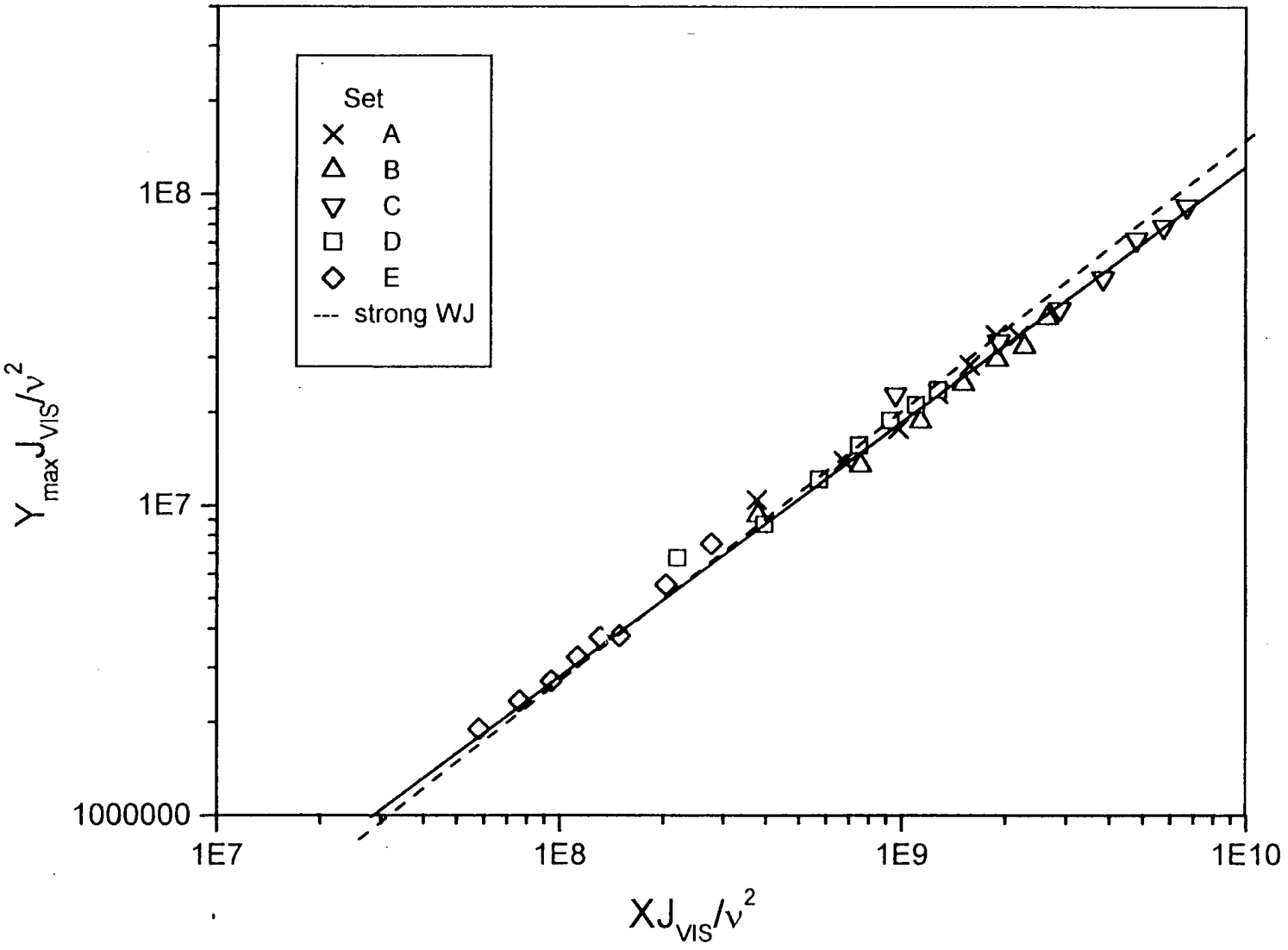


Fig.8. Scaling of $Y_{max}$ in the far field of type 1 weak wall jet

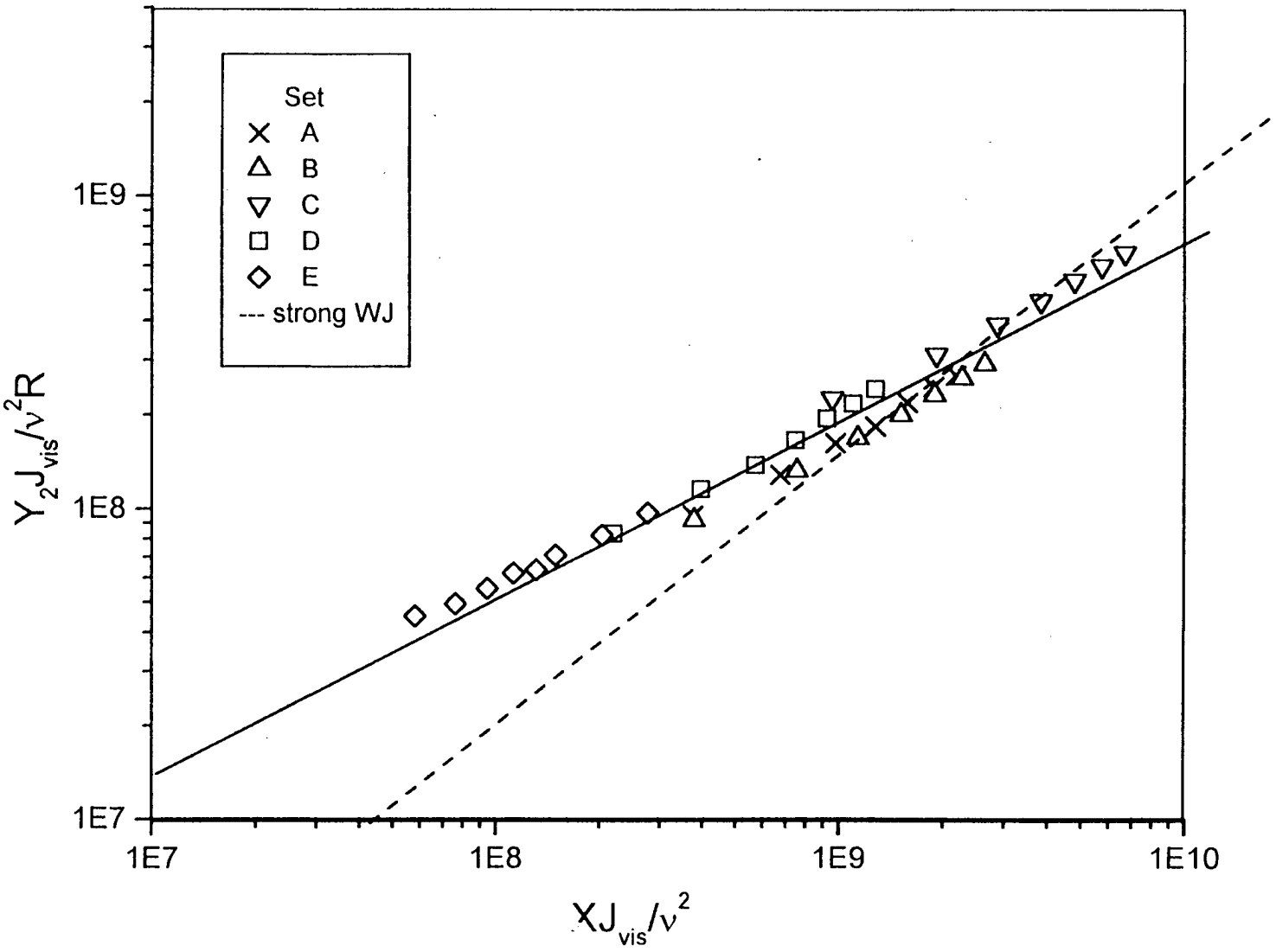


Fig9. Scaling of $Y_2$ in the far field of type 1 weak wall jet

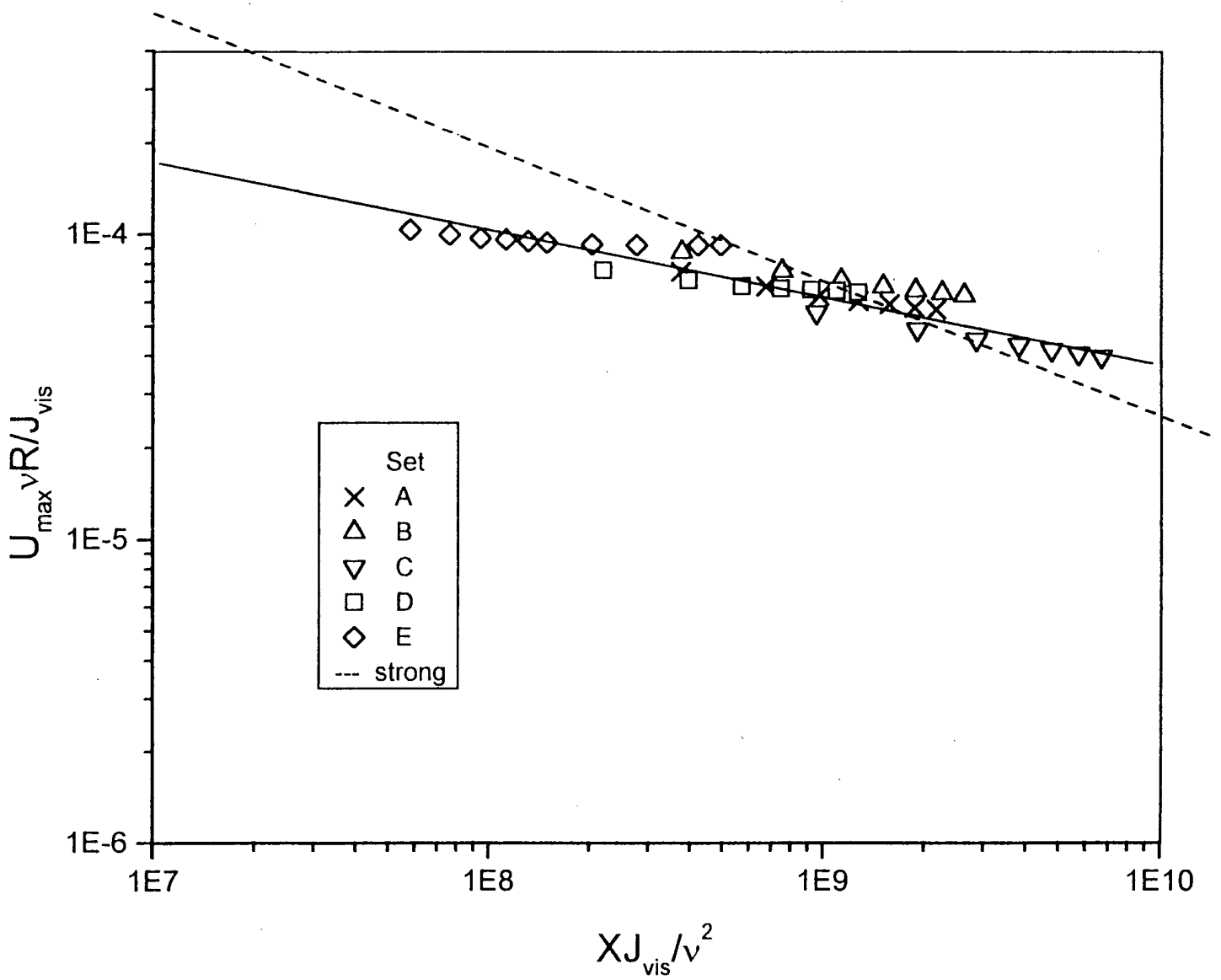


Fig.10. Scaling of $U_{max}$ in the far field of type 1 weak wall jet.

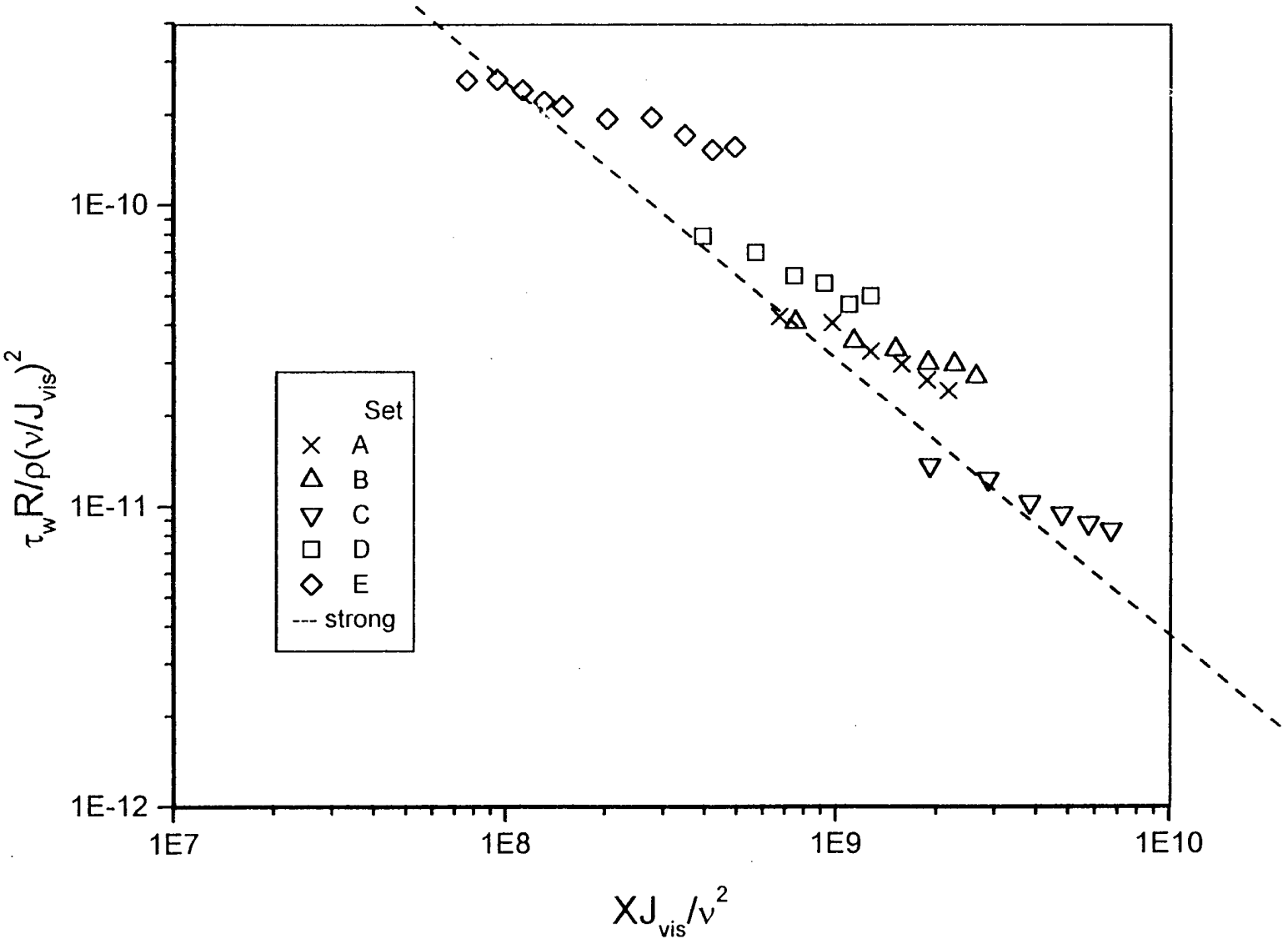


Fig.11 Scaling of skin friction in the far field of type 1 weak wall jet without considering the Reynolds number effect.

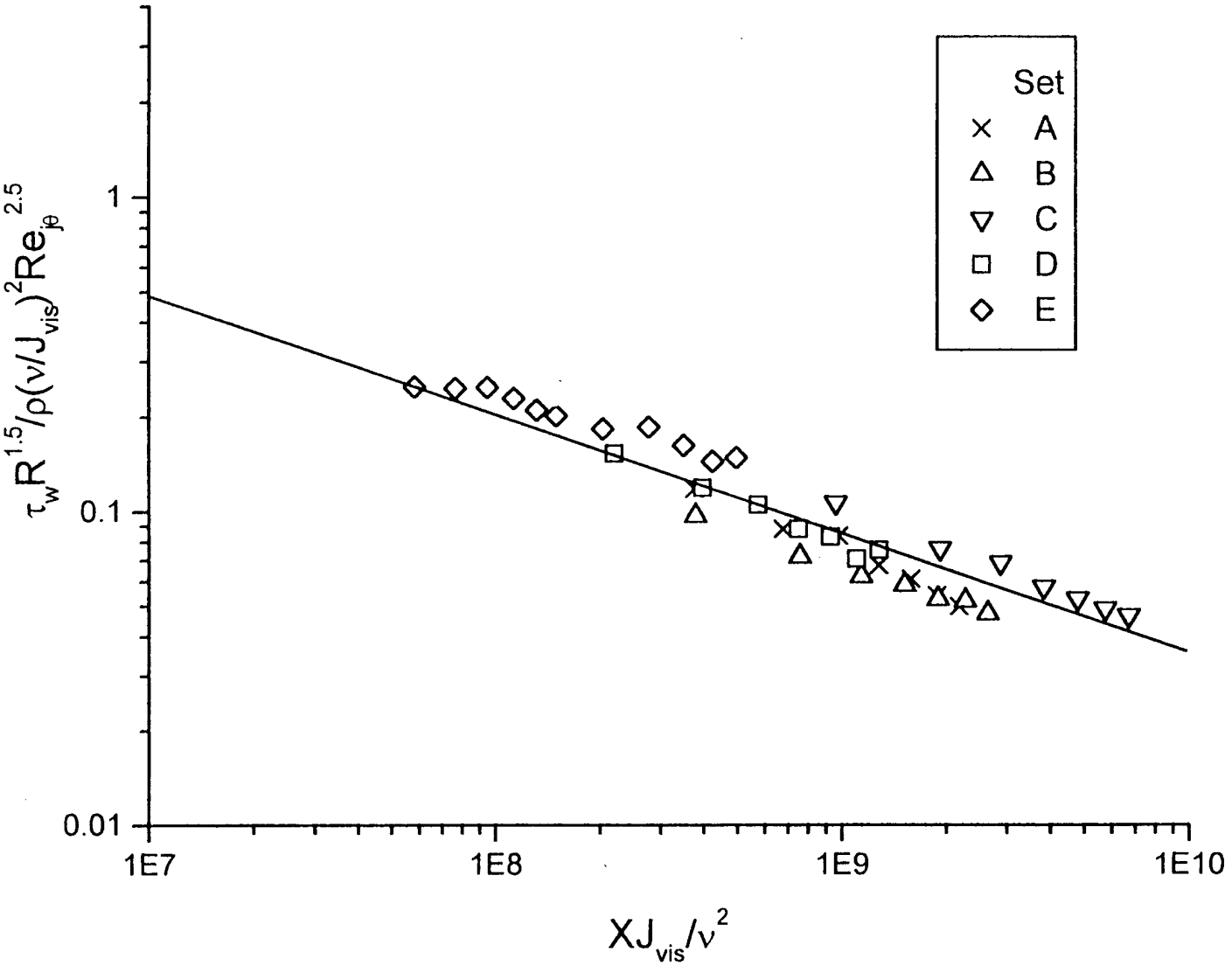


Fig.12. Scaling of skin friction in the far field of type 1 weak wall jet considering the Reynolds number effect.

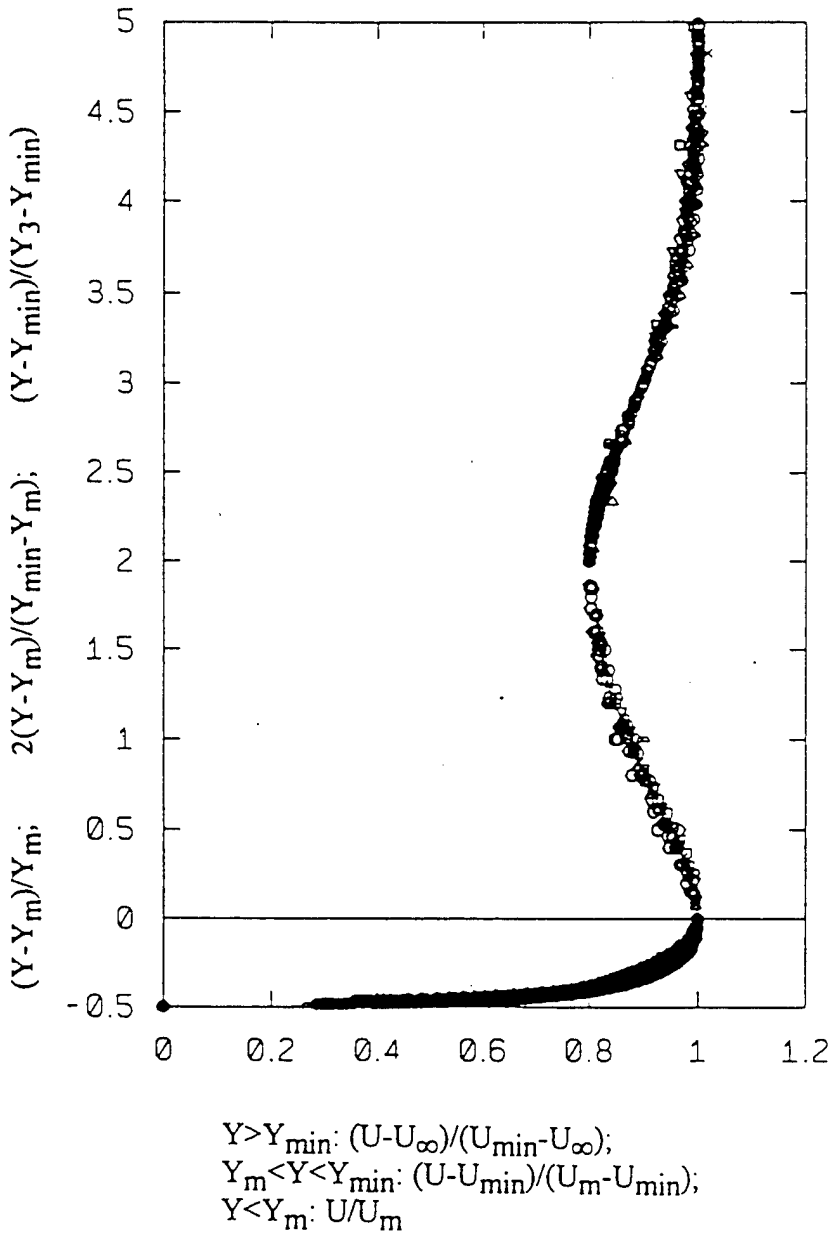


Fig.13. Mean velocity profiles in the near field of weak wall jets normalized with three velocity scales and three length scales.

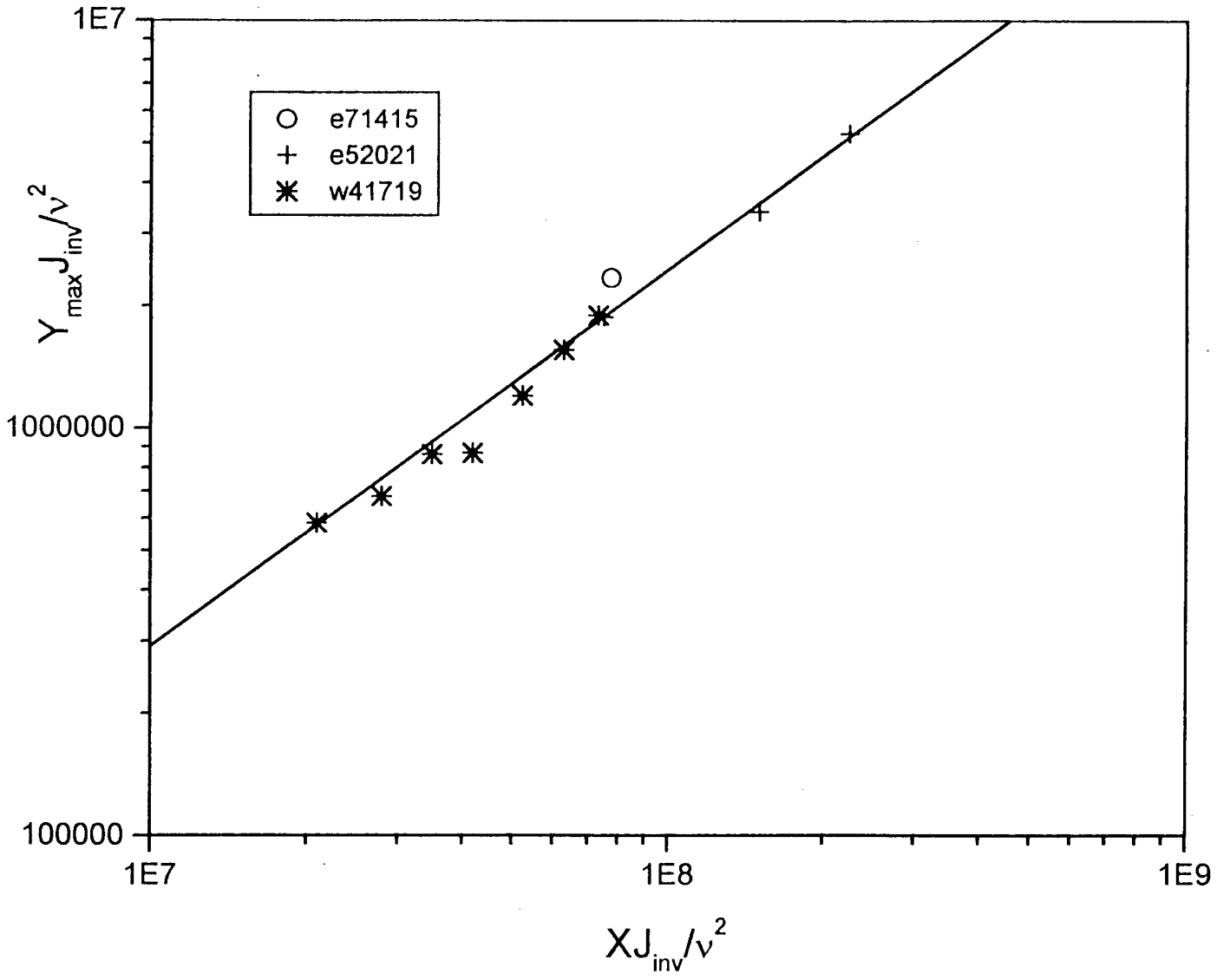


Fig.14. Scaling of $Y_{max}$ in the near field of type 2 weak wall jet.

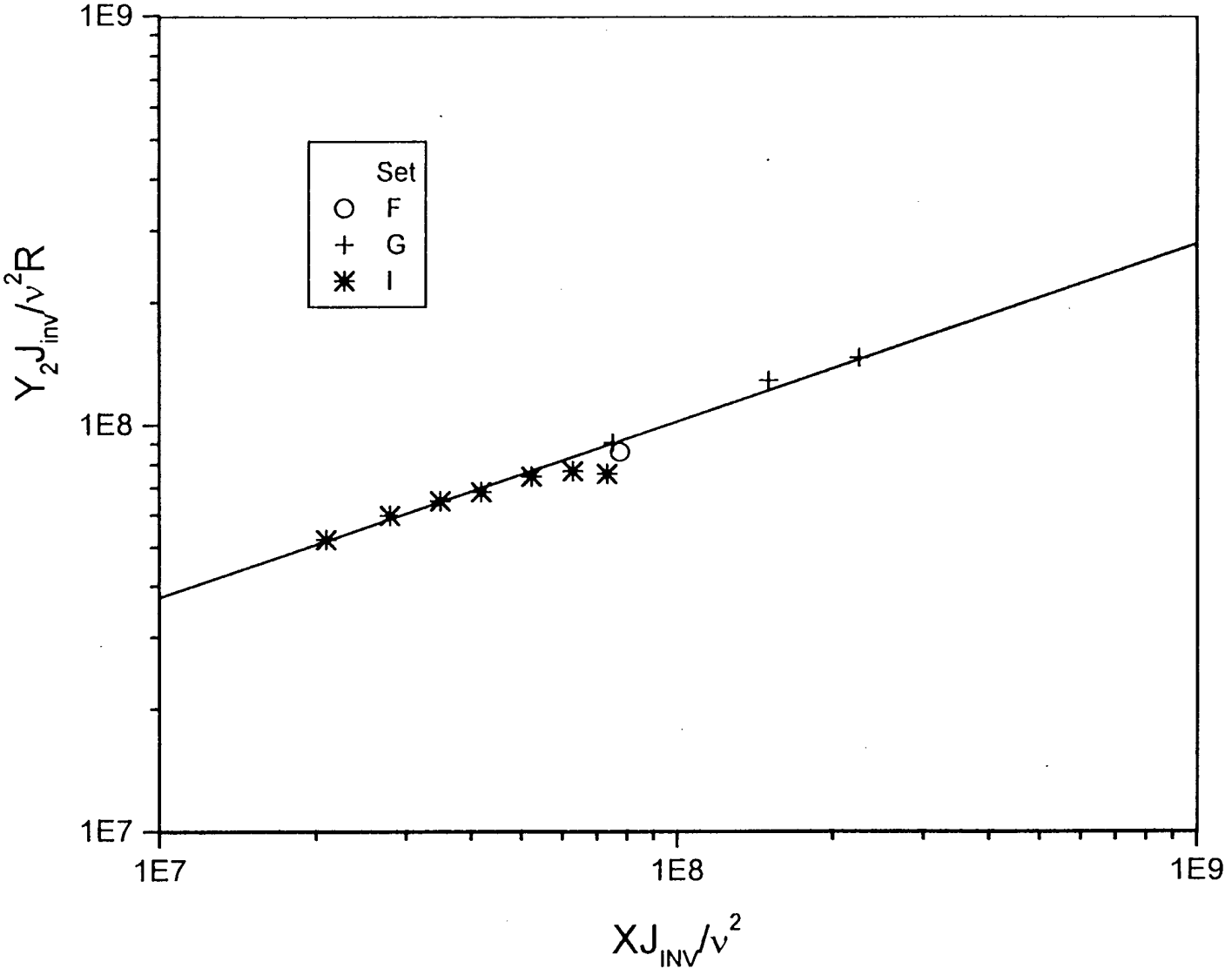


Fig.15. Scaling of $Y_2$ in the near field of type 2 weak wall jet.

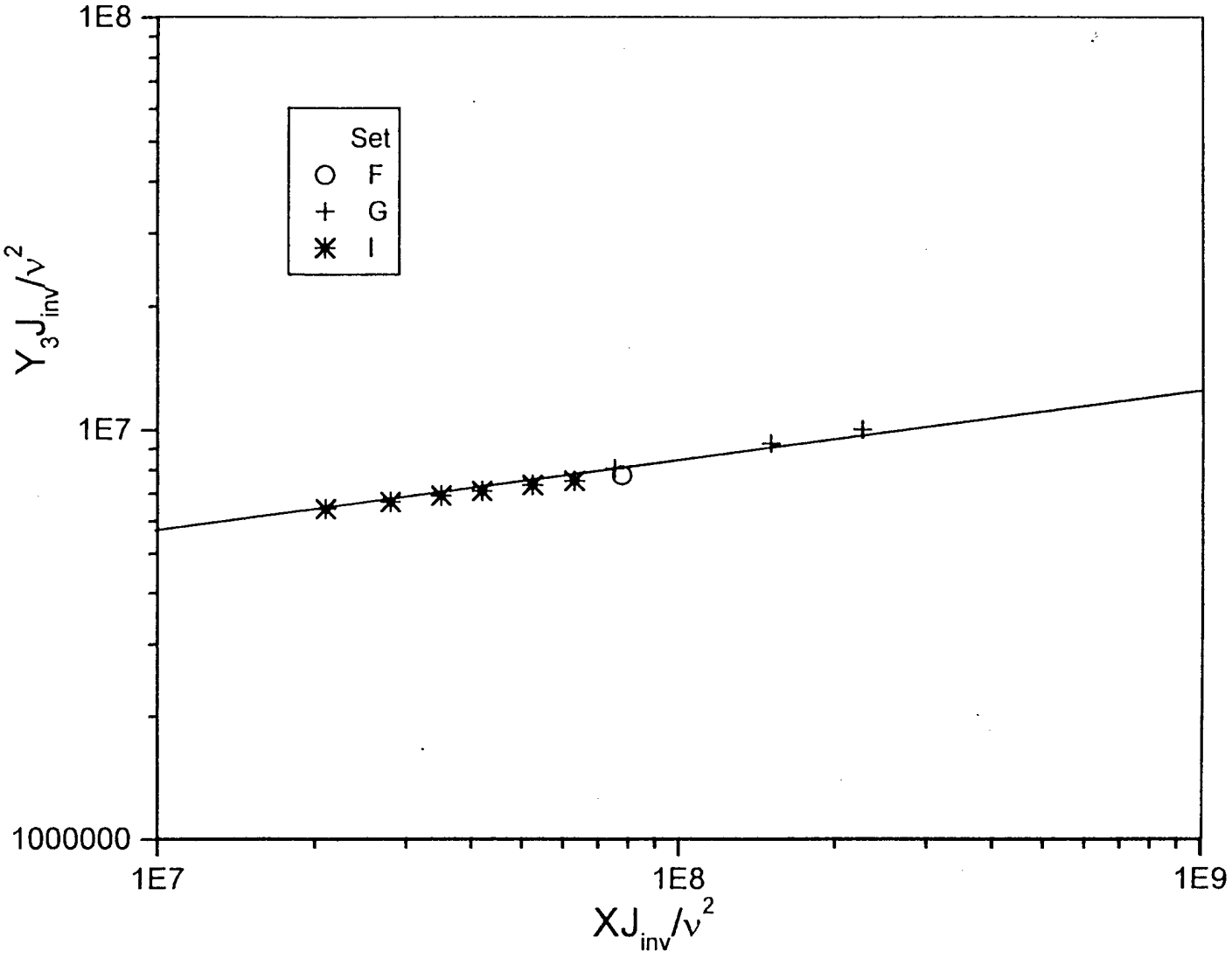


Fig.16. Scaling of $Y_3$ in the near field of type 2 weak wall jet.

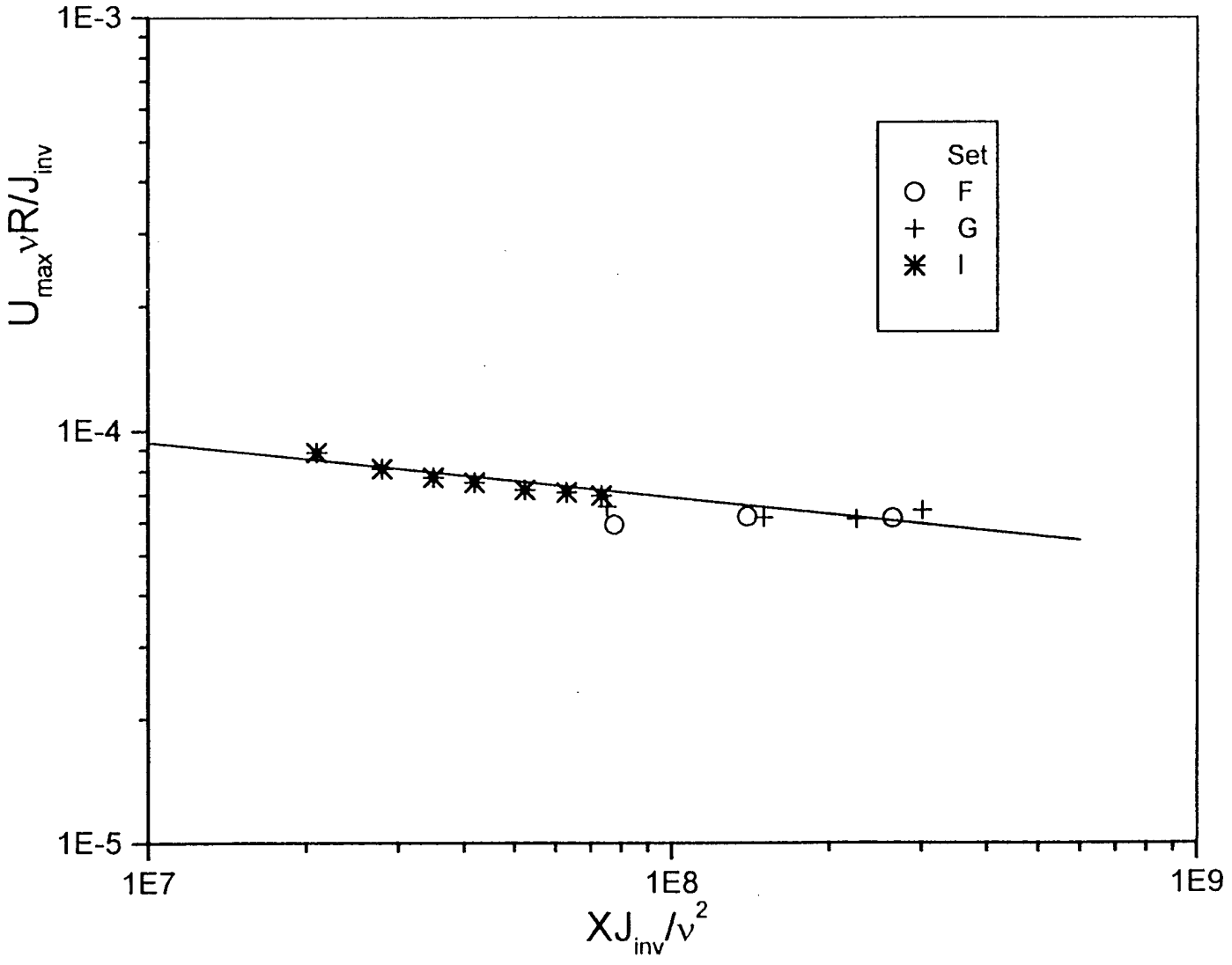


Fig.17. Scaling of $U_{max}$ in the near field of type 2 weak wall jet.

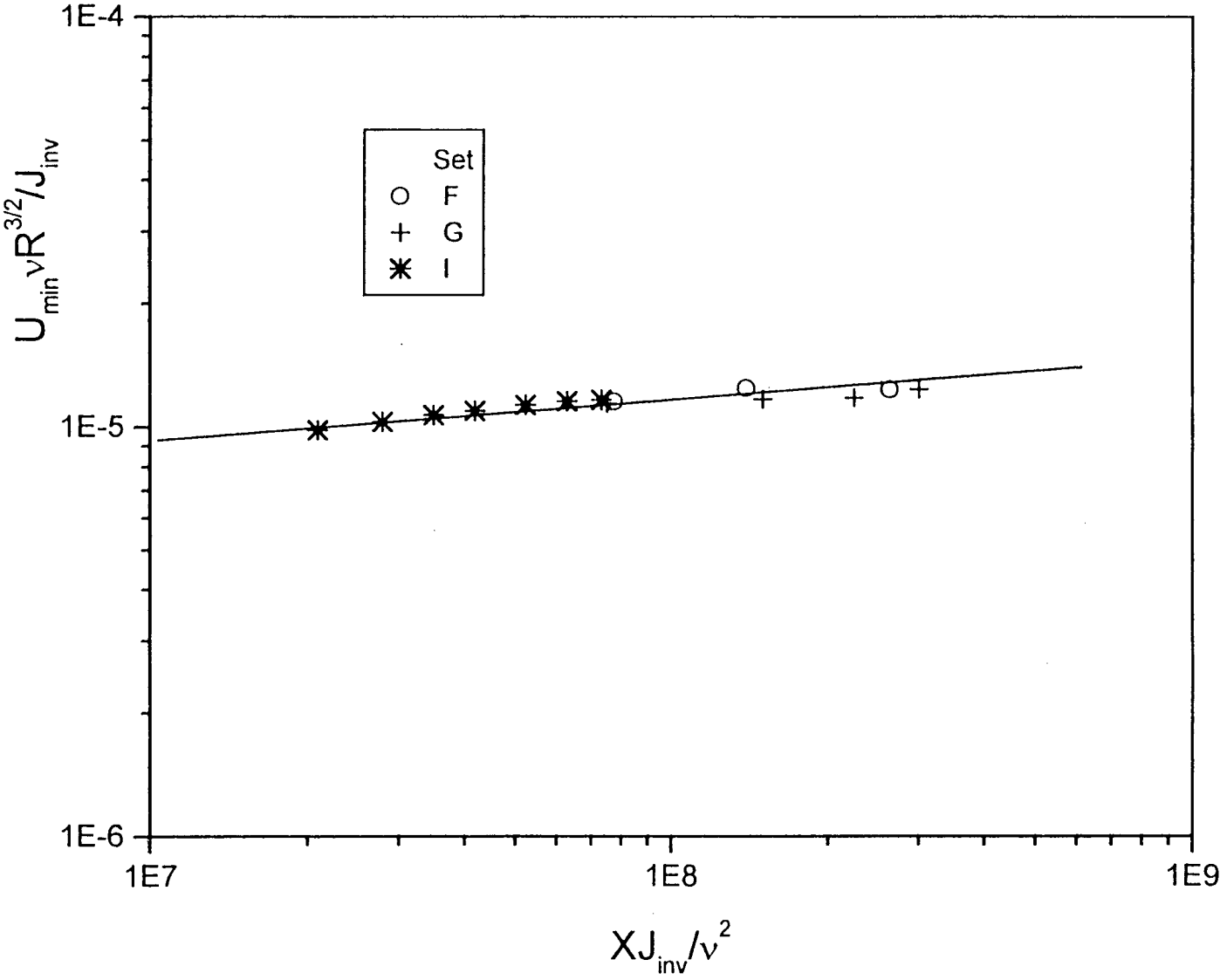


Fig. 18. Scaling of $U_{min}$ in the near field of type 2 weak wall jet.

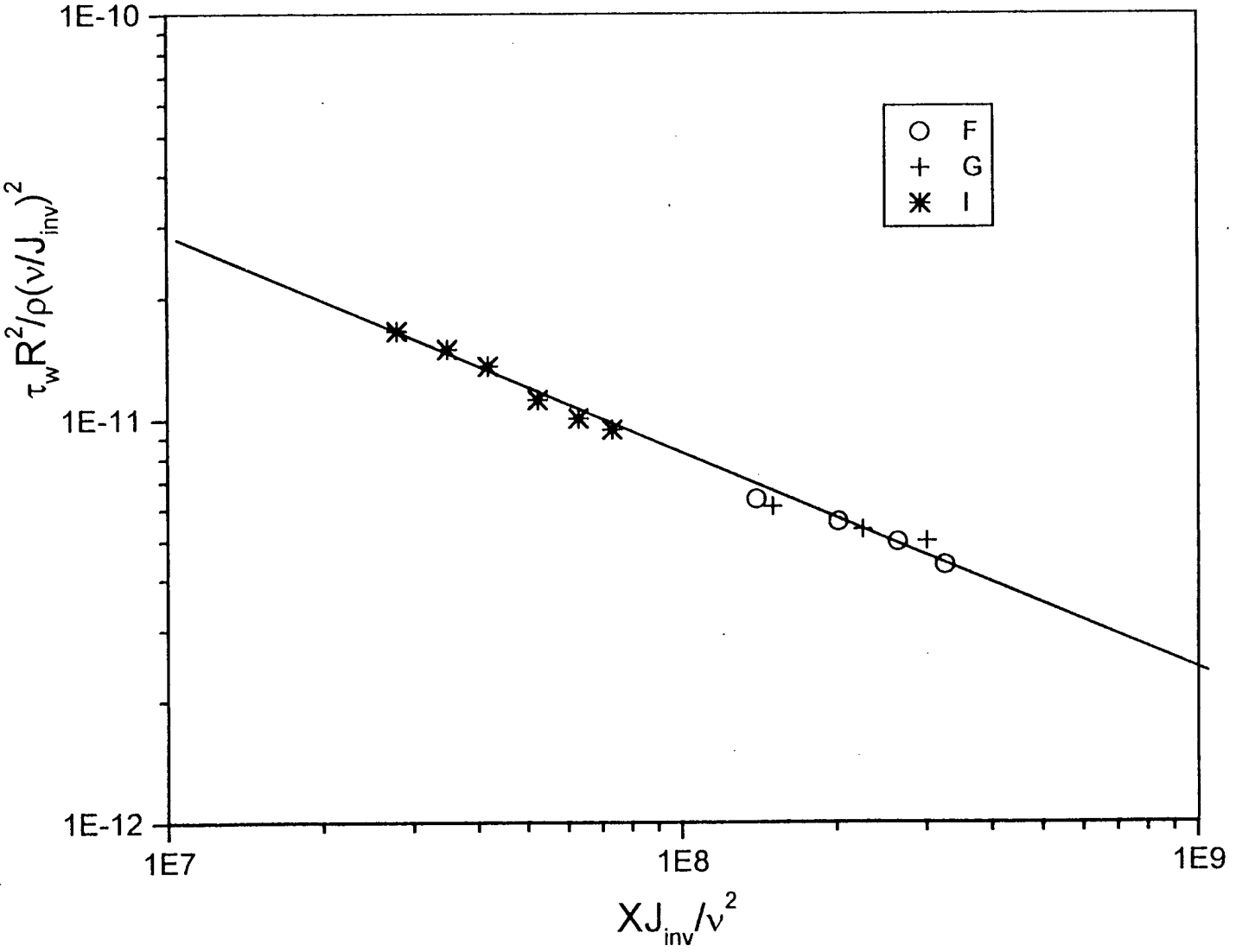


Fig.19. Scaling of skin friction in the near field of type 2 weak wall jet.

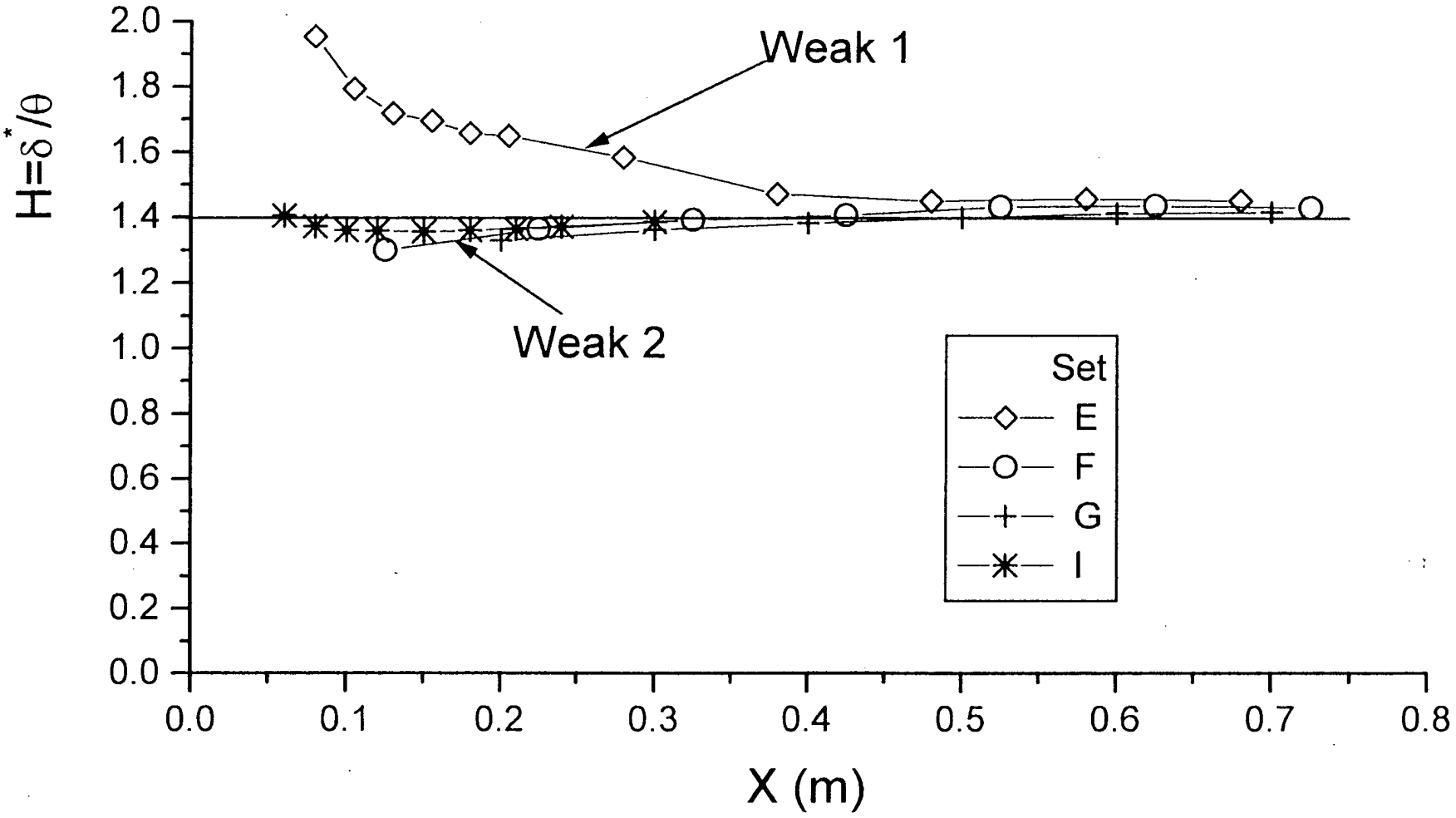


Fig.20. Streamwise development of the shape factor in the type 2 weak wall jet

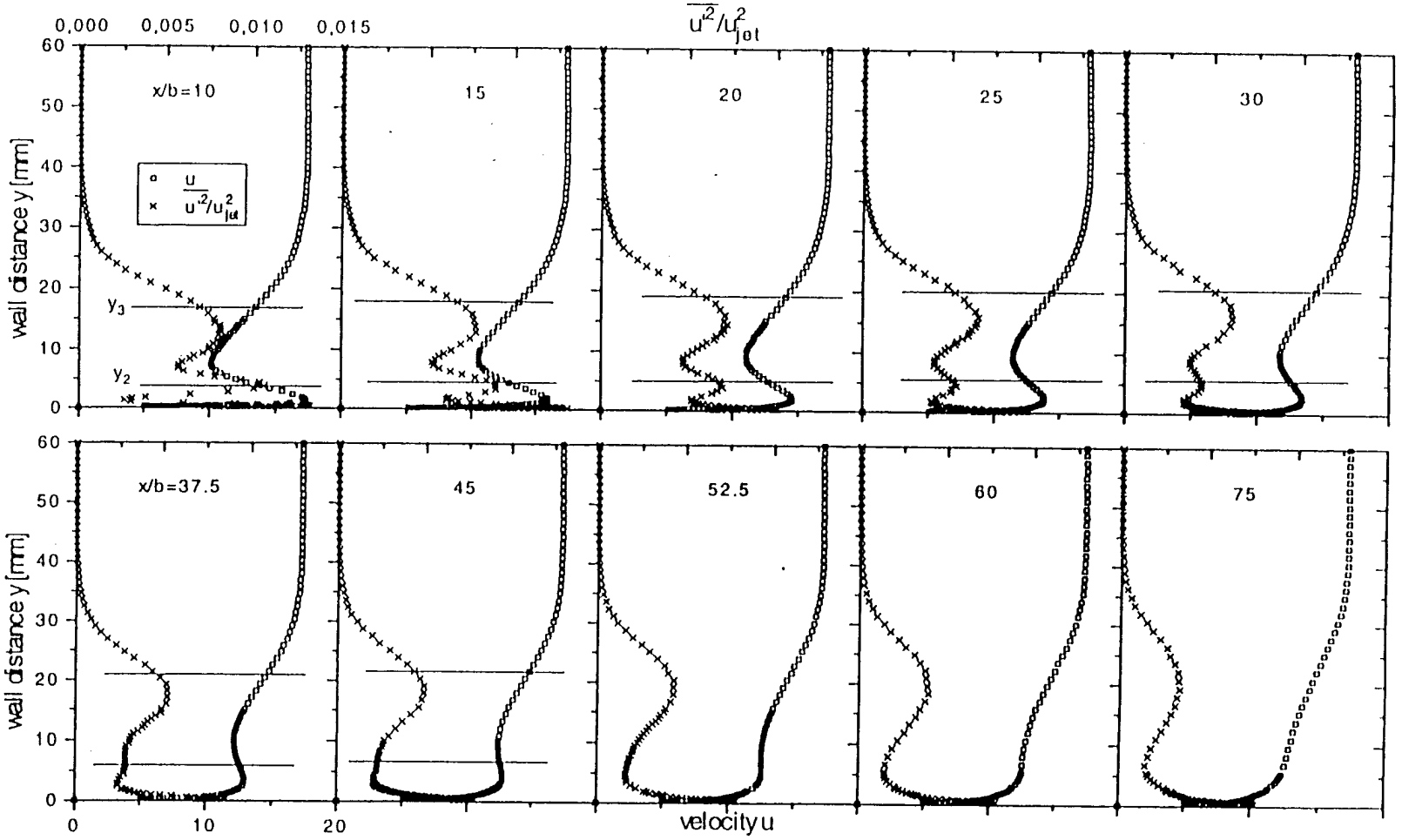


Fig.21. Mean velocity and turbulence energy distribution of a selected type 2 weak wall jet (data set I)

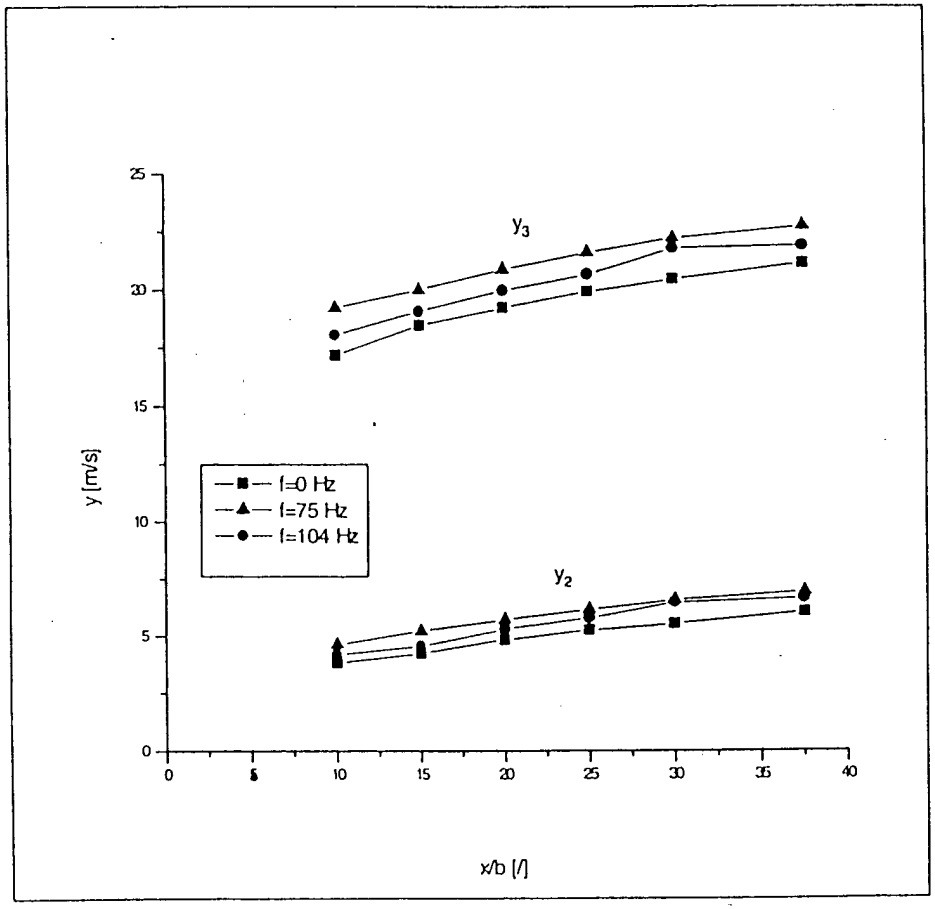


Fig.22. Influence of external excitation on the spreading of a weak wall jet (data set I, K and L).

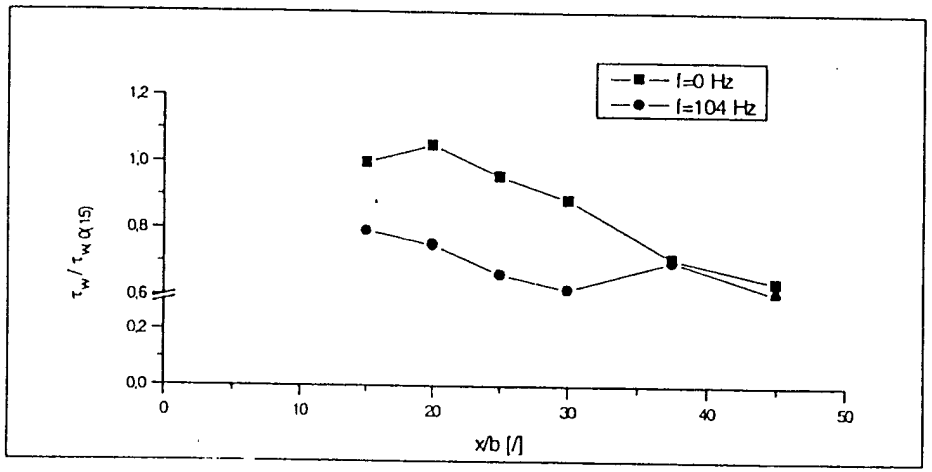


Fig.23. Influence of external excitation on the skin friction Cf (data set K).

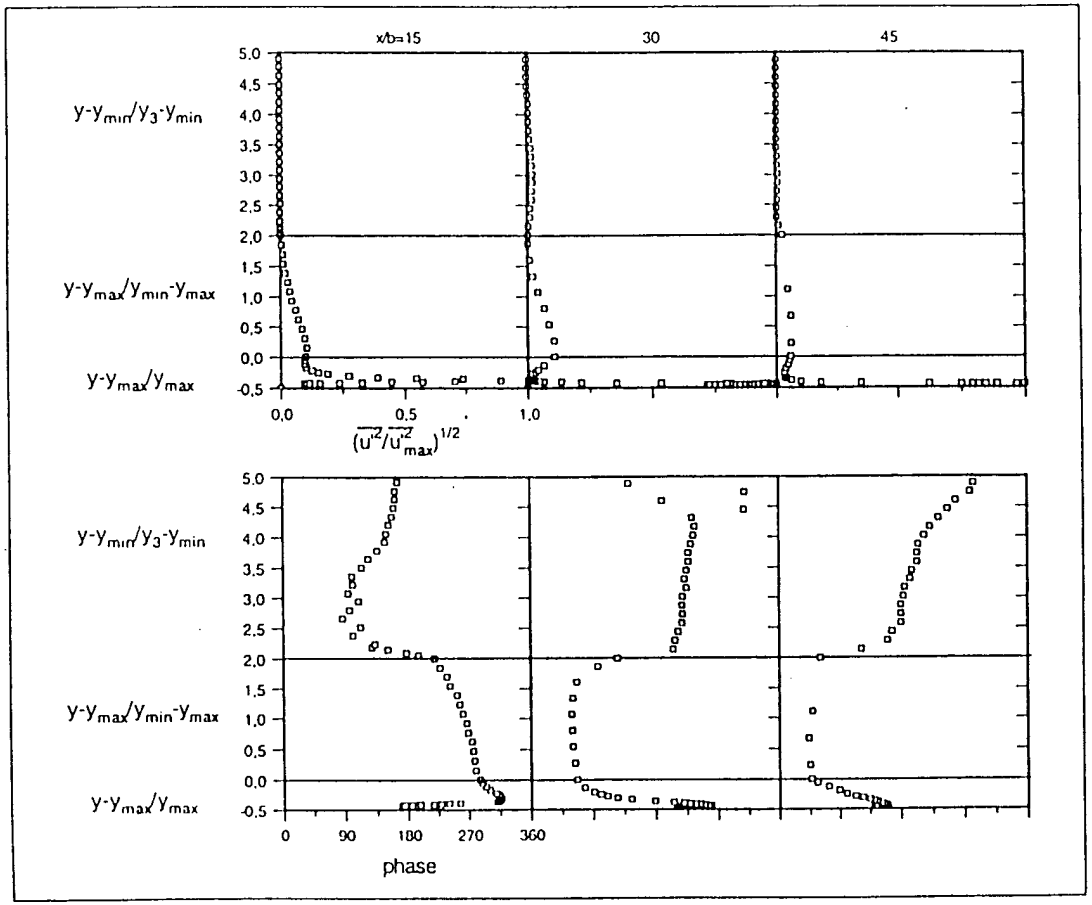


Fig.24. Amplitude and phase distributions under forcing at the inner instability frequency obtained by the phase locked ensemble averaging technique (data set K).

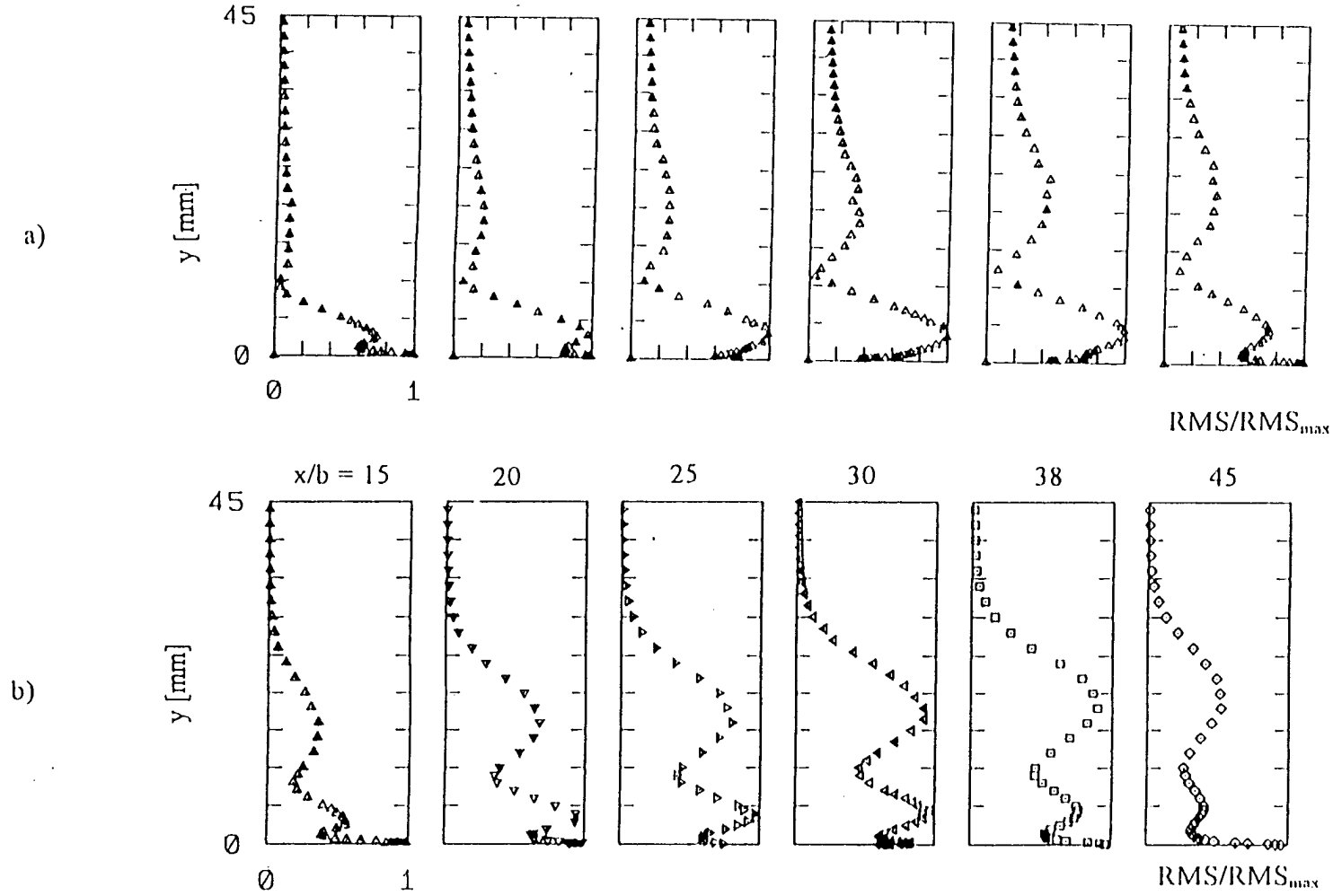


Fig.25. Coherent amplitude distribution with forcing at the middle instability frequency (data set L).

a. Amplitude distributions obtained by the phase locked ensemble averaging technique

b. Amplitude distribution obtained by the temporal pattern matching technique.

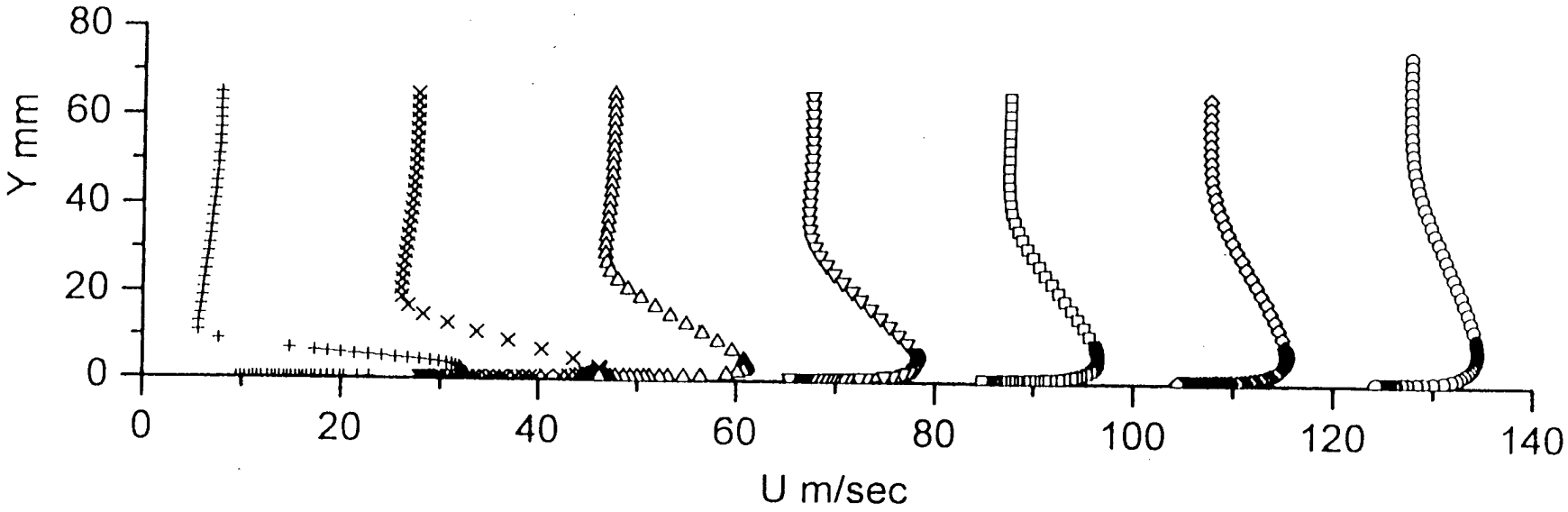


Uinf=8m/s, Uj=33m/m, b=5mm, θ=8.61mm

Fig.26. A strong wall jet embedded in an artificially thickened boundary layer.

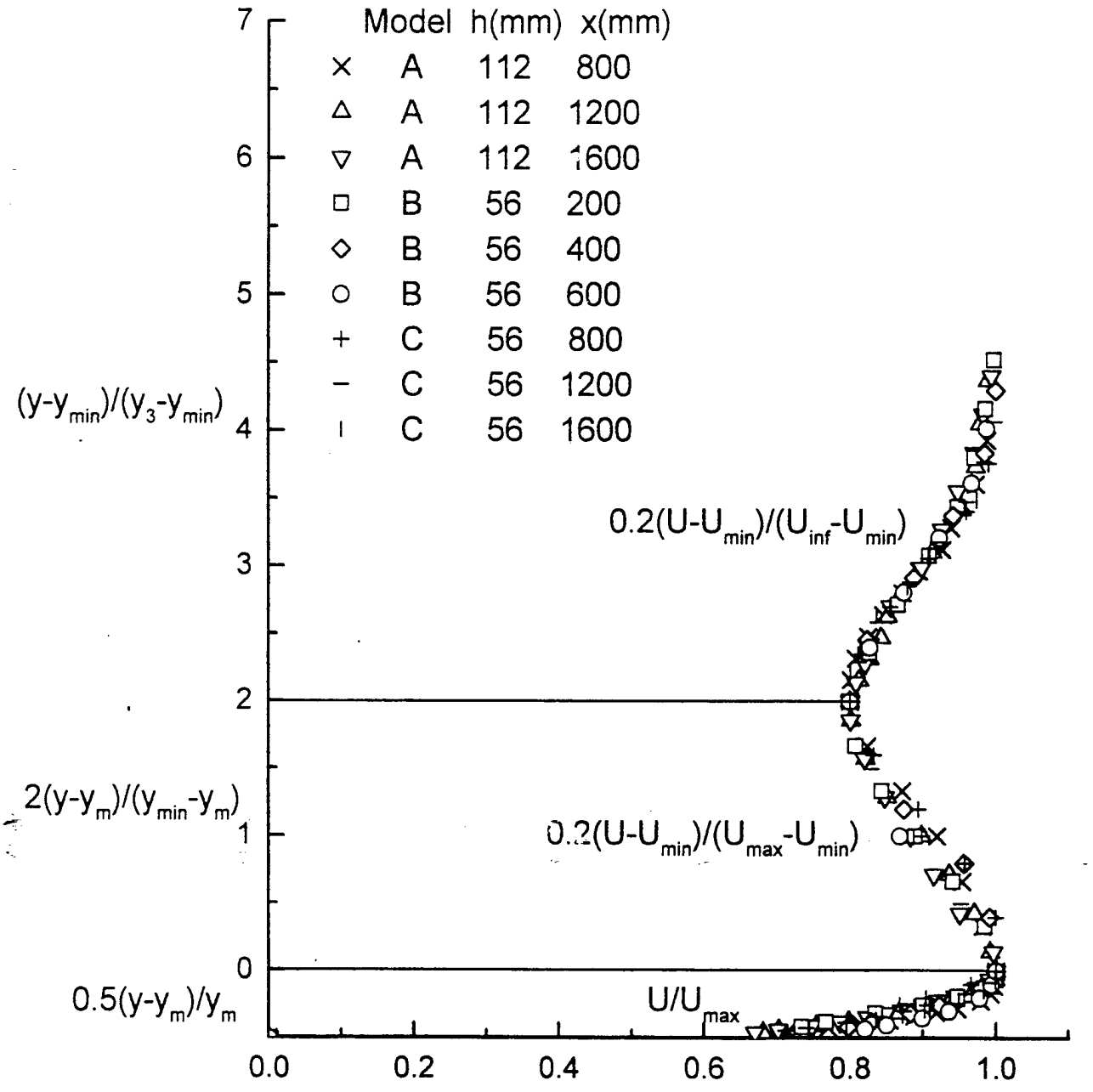


Fig.27. The mean velocity profiles of the wall wake normalized with three velocoty scales and three length scales.